

The Threshold $t\bar{t}$ Cross Section at NNLL Order

A. H. Hoang^a, A. V. Manohar^b, I. W. Stewart^b, and T. Teubner^c

^a *Max-Planck-Institut für Physik (Werner-Heisenberg-Institut),
Föhringer Ring 6, 80805 München, Germany*

^b *Department of Physics, University of California at San Diego,
9500 Gilman Drive, La Jolla, CA 92093-0319, USA*

^c *Institut für Theoretische Physik E, RWTH Aachen, D-52056 Aachen, Germany*

Abstract

The total cross section for top quark pair production close to threshold in e^+e^- annihilation is investigated. Details are given about the calculation at next-to-next-to-leading logarithmic order. The summation of logarithms leads to a convergent expansion for the normalization of the cross section, and small residual dependence on the subtraction parameter ν . A detailed analysis of the residual ν dependence is carried out. A conservative estimate for the remaining uncertainty in the normalization of the total cross section from QCD effects is $\delta\sigma_{t\bar{t}}/\sigma_{t\bar{t}} \lesssim \pm 3\%$. This makes precise extractions of the strong coupling and top width feasible, and further studies of electroweak effects mandatory.

I. INTRODUCTION

Detailed studies of the top quark are among the major projects of a future lepton pair collider. Of particular interest is the production of top quark pairs close to threshold, where the top quark velocity v is small and the usual perturbative expansion in terms of the strong coupling breaks down due to Coulomb singularities. The large top quark width $\Gamma_t \sim 1.5$ GeV prohibits the production of toponium states and leads to a cross section that rises smoothly when top pair production becomes kinematically allowed. Furthermore, the large decay rate, $\Gamma_t \gg \Lambda_{\text{QCD}}$, serves as an infrared cutoff, allowing the use of perturbative methods for the description of the non-relativistic top-antitop dynamics to a high degree of precision [1, 2].

In the past numerous studies have been carried out to assess the feasibility and precision for extracting various top quark properties from a threshold run [3–9]. Recently, next-to-next-to-leading order (NNLO) QCD corrections to the total cross section were calculated using the concept of effective field theories [10–16]. Surprisingly, the corrections were found to be as large as the next-to-leading order (NLO) QCD corrections. From the residual scale dependence in the NNLO result, the normalization of the cross section was estimated to have $\approx 20\%$ uncertainty [17]. It was concluded that top quark short-distance mass parameters can be determined with a precision of 200 MeV or better from the shape of the cross section, if so-called threshold mass parameters are employed [17, 18]. However, the large NNLO QCD corrections to the normalization of the cross section seemed to jeopardize competitive measurements of the top width, strong top coupling [18], or the top Yukawa coupling in the case of a light Higgs. Moreover, the large NNLO corrections seemed to indicate that, despite the perturbative nature of the $t\bar{t}$ system, high precision computations are not feasible.

A common feature of all the NNLO QCD calculations is that the running from the hard scale m_t down to the non-relativistic scales which govern the dynamics of the top-antitop system was not taken into account. In other words, at NNLO potentially large QCD logarithms of ratios of the hard scale and the non-relativistic scales $m_t v$ and $m_t v^2$ were treated perturbatively. From weak decays of K and B mesons, it is known that a consistent summation of logarithms between m_W and the low-energy hadronic scales can significantly change the magnitude of Wilson coefficients and the corresponding physical predictions (see for e.g. Ref. [19]). In the case of the top quarks near threshold all the scales are well separated, $m_t \gg m_t v \gg m_t v^2 \gg \Lambda_{\text{QCD}}$. Since $\ln[m_t/(m_t v^2)] \sim \ln(40) = 3.7$, these logarithmic contributions can be sizeable (see for e.g. Ref. [20]).

In this work details are presented for the computation in Ref. [21] where the impact of the summation of QCD logarithms of v on the photon induced total cross section were examined. We also add the vector and axial-vector contributions from Z exchange. In this framework the expansion for the normalized cross section R takes the form

$$R = \frac{\sigma_{t\bar{t}}}{\sigma_{\mu^+\mu^-}} = v \sum_k \left(\frac{\alpha_s}{v}\right)^k \sum_i (\alpha_s \ln v)^i \times \left\{ 1 \text{ (LL)}; \alpha_s, v \text{ (NLL)}; \alpha_s^2, \alpha_s v, v^2 \text{ (NNLL)} \right\}, \quad (1)$$

where the indicated terms are of leading logarithmic (LL), next-to-leading logarithmic (NLL), and next-to-next-to-leading logarithmic (NNLL) order. The summation of logarithms can be performed using renormalization group equations in the framework of “velocity NRQCD” (vNRQCD) [22–25], an effective theory for heavy quark pairs. The logarithmic corrections treated in this work are at NNLL order and fully include the known NNLO QCD

corrections from Refs. [10–16]. A complete summation requires knowledge of the Wilson coefficients for potentials and non-relativistic production currents at this order. For the NNLL potentials the required Wilson coefficients have been calculated in Refs. [23, 25, 26]. The LL running of subleading $t\bar{t}$ production currents is also required and is given below. For the leading production current the Wilson coefficient is known at NLL [25] and NNLO [27–29]. For this current only partial NNLL results are known and an estimate is made for the uncertainty this induces in our result. The combination of known NNLL results significantly reduces the size and scale dependence of previous NNLO QCD predictions [17].

We emphasize that we do not treat electroweak effects consistently at the same level as the QCD corrections, as implied by the counting $\Gamma_t \sim m_t v^2$ used in this paper. This would require the inclusion of non-factorizable corrections as well as the single- and non-resonant background contributions, which is beyond the scope of this work. Here we only include the top quark width through an imaginary mass term, which can be implemented by the replacement [2], $E \equiv \sqrt{s} - 2m_t \rightarrow E + i\Gamma_t$ into a calculation for stable quarks. For the total cross section this represents a consistent next-to-leading order treatment of electroweak effects [30]. We stress, however, that with the small uncertainties in R resulting from our NNLL QCD results, a systematic treatment of higher order electroweak related effects is desirable.

The outline of the paper is as follows. In section II we review an example from inclusive non-leptonic B -decays to emphasize some important differences between fixed order and renormalization group improved calculations. In section III we discuss the matching and running of Wilson coefficients for top quark production near threshold. In section IV we evaluate the time ordered products of currents at the endpoint of the renormalization group evolution. Pole mass results are given in section V, while our implementation of the 1S mass is presented in section VI. In section VII the NNLL 1S mass results are presented and the remaining theoretical uncertainty is analyzed. The consequences of our results for measurements of the top width, $\alpha_s(m_Z)$, and the Higgs top Yukawa coupling are discussed in section VIII, followed by conclusions in section IX.

II. SUMMING LOGARITHMS

To outline the steps in our renormalization group improved calculation it is instructive to draw a parallel with the well-known computation for inclusive non-leptonic \bar{B} -meson decays via the quark decay $b \rightarrow c\bar{u}d$. This process involves several scales — m_W , m_b , m_c and Λ_{QCD} , but only m_W and m_b will be discussed here. The relevant weak decay Hamiltonian at the scale μ is

$$H_W = \frac{4G_F}{\sqrt{2}} V_{cb} V_{ud}^* \left[C_1(\mu) O_1(\mu) + C_2(\mu) O_2(\mu) \right], \quad (2)$$

$$O_1(\mu) = [\bar{c}^\alpha \gamma_\mu P_L b_\alpha] [\bar{d}^\beta \gamma^\mu P_L u_\beta], \quad O_2(\mu) = [\bar{c}^\beta \gamma_\mu P_L b_\alpha] [\bar{d}^\alpha \gamma^\mu P_L u_\beta],$$

where $P_L = (1 - \gamma_5)/2$. H_W is μ -independent and the μ dependence of $C_i(\mu)$ is compensated by the μ dependence of $O_i(\mu)$. The coefficients $C_{1,2}(m_W)$ are determined by integrating out W bosons in the $b \rightarrow c\bar{u}d$ amplitude at $\mu = m_W$

$$C_1(\mu = m_W) = 1 + \mathcal{O}(\alpha_s(m_W)), \quad C_2(\mu = m_W) = 0 + \mathcal{O}(\alpha_s(m_W)). \quad (3)$$

The coefficients can be computed using perturbation theory in $\alpha_s(m_W)$, which is valid as long as $\alpha_s(m_W)$ is small. There are no large logarithms in the matching calculation since we have chosen $\mu = m_W$. The decay amplitude can then be computed by taking the matrix elements of $O_1(\mu = m_W)$ in the \bar{B} -meson. The problem is that these matrix elements contain large logarithms of m_W/m_b . Using the renormalization group these large logarithms can instead be moved into the coefficients C_i and summed by scaling O_i and C_i from $\mu = m_W$ to $\mu = m_b$. Note that in a fixed order expansion without the renormalization group large logarithms exist even for $\mu = m_b$. The renormalization group equation (RGE) for the coefficients is

$$\mu \frac{d}{d\mu} C_i = \gamma_{ji} C_j, \quad \gamma(g) = \frac{g^2}{8\pi^2} \begin{bmatrix} -1 & 3 \\ 3 & -1 \end{bmatrix} + \mathcal{O}(g^4), \quad (4)$$

and is diagonalized by taking $C_{\pm} = C_1 \pm C_2$. Provided the strong coupling $\alpha_s(\mu)$ is small over the integration range in Eq. (4), higher order terms in γ and β can be neglected and

$$C_{\pm}(\mu) = \left[\frac{\alpha_s(m_W)}{\alpha_s(\mu)} \right]^{a_{\pm}}, \quad a_+ = \frac{2}{\beta_0}, \quad a_- = -\frac{4}{\beta_0}. \quad (5)$$

Using $\alpha_s(m_W) = 0.12$ and $\alpha_s(m_b) = 0.22$ the coefficients C_{\pm} at $\mu = m_b$ are

$$C_+(m_b) = 0.85, \quad C_-(m_b) = 1.37, \quad (6)$$

a change of -15% and 37% from their values at m_W . Finally, the inclusive \bar{B} meson decay rate is computed from the imaginary part of the matrix element of a time-ordered product, $\langle \bar{B} | i \int d^4x T H_W^\dagger(x) H_W(0) | \bar{B} \rangle$. At leading order in $1/m_b$ at the scale $\mu = m_b$, the operator product expansion gives [31]

$$\Gamma^{\Delta c=1} = \frac{3G_F^2 m_b^5}{192\pi^3} |V_{cb}V_{ud}|^2 \left(C_1^2(m_b) + \frac{2}{3} C_1(m_b) C_2(m_b) + C_2^2(m_b) \right) f(m_c^2/m_b^2), \quad (7)$$

where $f(m_c^2/m_b^2)$ is a phase-space factor. The QCD corrections to this resummed result are of order $\alpha_s(m_b)$ with no large logarithm.

In the above example the computation of the decay rate was divided into three parts:

1. Compute the coefficients $C_i(\mu = m_W)$ in a perturbation series in $\alpha_s(m_W)$, which is valid as long as $\alpha_s(m_W)$ is small.
2. Scale $C_i(\mu)$ from $\mu = m_W$ to $\mu = m_b$ using the renormalization group, which can be done provided $\alpha_s(\mu)$ is small in the region $m_b \leq \mu \leq m_W$. This scaling sums terms of the form $[\alpha_s \ln(m_b/m_W)]^k$. The terms neglected in the anomalous dimension are smaller than those retained by $\alpha_s(\mu)$ at all points in the integration region.
3. Compute the decay rate using H_W renormalized at $\mu = m_b$ in a perturbation series in $\alpha_s(m_b)$ (and $1/m_b$), which is valid as long as $\alpha_s(m_b)$ is small.

Since $\alpha_s(\mu)$ is monotonically increasing as μ decreases, all three steps above are valid as long as $\alpha_s(m_b)$ is small. However, it is crucial to note that because of the renormalization group improvement we do not need to assume that

$$\alpha_s(m_W) \ln \left[\frac{m_W^2}{m_b^2} \right] \simeq 0.7 \quad (8)$$

is a small expansion parameter. In contrast, a fixed order computation of the decay rate in powers of $\alpha_s(\mu)$ contains logarithms of m_W/μ and m_b/μ , and is valid only if $\alpha_s(\mu)$ times these logarithms is small. In particular, one needs $\alpha_s(m_b) \ln(m_W^2/m_b^2)$ to be small. As a result, fixed order calculations have limited validity when processes involve widely separated scales.

For non-relativistic top quarks the running spans an even larger range of energies than the above example, $\mu = m_t$ down to $\mu = m_t v^2 \sim 4 \text{ GeV}$. Therefore, at the order that anomalous dimensions depend directly on the $m_t v^2$ energy scale (NNLO), it is not too surprising that renormalization group improved perturbation theory is necessary to compute the $t\bar{t}$ cross-section. Since $E \sim 4 \text{ GeV}$, fixed order perturbation theory would be valid only if

$$\alpha_s(m_t) \ln \left[\frac{m_t^2}{E^2} \right] \simeq 0.8 \quad (9)$$

were small. In contrast to Eq. (9), renormalization group improved perturbation theory only requires $\alpha_s(m_t v^2)$ to be small. Relative to B -decays the radiative corrections for top quark production could be even larger, since factors of α_s for the bound state do not always come with a $1/\pi$. This is true of both the constant and logarithmically enhanced terms.

For the highest order computed, fixed order perturbation theory cannot distinguish the scale at which to evaluate α_s . Mistaking an $\alpha_s(m_t)$ for an $\alpha_s(m_t v^2)$ is a difference of a factor of two. Renormalization group improved perturbation theory distinguishes the α_s 's that appear at each order. We note that in our NNLL order results, the summation of logarithms which involve the $m_t v^2$ scale do tend to numerically dominate.

III. EFFECTIVE THEORY

For our calculation we will employ vNRQCD [22–25], an effective field theory which describes the non-relativistic dynamics of heavy quark pairs, where the non-relativistic scales mv (momentum) and mv^2 (energy) are larger than the hadronization scale Λ_{QCD} , m being the heavy quark mass. This effective theory contains a consistent power counting in v , so that a given Feynman diagram contributes to a single order in the v expansion. It also accounts for the fact that the momentum (soft) and the energy (ultrasoft) scales are correlated through the heavy quark equations of motions. Finally, vNRQCD allows for the summation of logarithms of ratios of the hard scale m and the non-relativistic scales using a velocity renormalization group. The most important momentum regions for heavy quark processes are those with (energy, momentum) that are hard (m, m) , soft (mv, mv) , potential (mv^2, mv) , and ultrasoft (mv^2, mv^2) [32]. The effective theory is formulated by including only those quark and gluonic degrees of freedom which can become on-shell for scales below m . The on-shell degrees of freedom are gluons and massless quarks with soft and ultrasoft energies and momenta, and heavy quarks with potential energies and momenta. All off-shell effects such as those from hard quarks and gluons, potential gluons, and soft quarks are accounted for by on-shell matching of vNRQCD to full QCD at the hard scale.

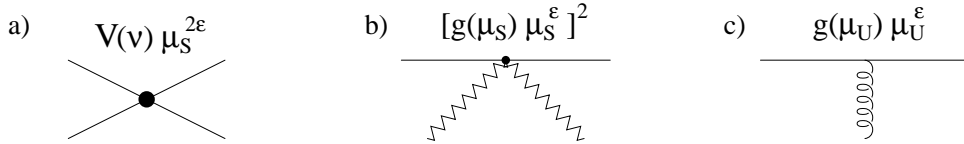


FIG. 1. Examples of potential (a), soft (b), and ultrasoft (c) interactions in vNRQCD.

Only ultrasoft energies and momenta are treated as continuous variables, and ultrasoft momenta are separated from larger momenta by employing the multipole expansion. Soft energies and momenta appear as discrete indices for potential quarks and soft gluons and must be summed over, similar to the velocity index v^μ for the static quark in HQET [31]. For instance, the first few terms that are bilinear in the quark field $\psi_{\mathbf{p}}$ are

$$\mathcal{L}(x) = \sum_{\mathbf{p}} \psi_{\mathbf{p}}^\dagger(x) \left\{ i\partial^0 - \frac{\mathbf{p}^2}{2m} + \frac{\mathbf{p}^4}{8m^3} \right\} \psi_{\mathbf{p}}(x), \quad (10)$$

where m is the pole mass, and there is a similar equation for the anti-quark field $\chi_{\mathbf{p}}$. Sums over soft and potential energies and momenta in combination with ultrasoft integrations in loop integrals can be rewritten as continuous loop integrals of soft and potential energies and momenta. The vNRQCD Lagrangian also contains operators that describe potential-type 4-quark interactions (Fig. 1a) originating from potential gluons and other off-shell modes, interactions of quarks with soft gluons (Fig. 1b), and ultrasoft gluons (Fig. 1c), as well as self-interactions of soft and ultrasoft gluons. The potential and soft interactions depend non-locally on the soft indices, but are local in ultrasoft momenta. Gauge invariance in soft energies and momenta is recovered through reparameterization invariance. Loop integrals are regularized with dimensional regularization in $d = 4 - 2\epsilon$ dimensions using the $\overline{\text{MS}}$ subtraction scheme.

The crucial feature of vNRQCD is that the dimensional $\overline{\text{MS}}$ subtraction scale for loop integrations over soft and potential momenta is μ_S , whereas for loop integrations with ultrasoft momenta it is μ_U . Within dimensional regularization the two different subtraction scales are necessary to properly recover the full d -dimensional non-relativistic phase space [22]. Powers of $(\mu_U)^\epsilon$ and $(\mu_S)^\epsilon$ are determined uniquely by the interaction vertices [24] as shown in Fig. 1. Furthermore, the two scales are correlated, $\mu_S = m\nu$ and $\mu_U = m\nu^2$, where the dimensionless velocity subtraction point ν takes the role of the $\overline{\text{MS}}$ scaling parameter. The correlation between μ_S and μ_U is an inherent property of vNRQCD, since the energy and momentum scales are related through the quark equations of motion. For NRQED this correlation is necessary to reproduce through running the $(\ln \alpha)^k$, $k \geq 2$ contributions in Lamb shifts, hyperfine splittings and the corrections to the ortho- and para-positronium decay widths [33, 34]. The renormalization group equations for Wilson coefficients are determined in the canonical way with the exception that they are formulated in terms of the subtraction velocity ν .

Lowering ν to a scale v_0 of order the quark velocity sums all logarithms of the soft and ultrasoft scales into the Wilson coefficients of the vNRQCD operators. At NNLL order this includes logarithms originating from ultrasoft radiation effects. The $t\bar{t}$ state is predominantly

Coulombic, so $v_0 \simeq C_F \alpha_s \simeq 0.15\text{--}0.20$. Once ν is lowered to v_0 , power counting shows that matrix elements with ultrasoft gluons no longer have to be taken into account at NNLL for the description of a heavy quark pair. Thus, at $\nu = v_0$ the NNLL Green functions of a color singlet quark-antiquark system are described by the two-body Schrödinger equation with relativistic corrections.

In the remainder of this section we introduce the Wilson coefficients which are matched at the hard scale ($\nu = 1$), and run from $\nu = 1$ to v_0 .

A. Potentials

The potentials in the NNLL Schrödinger equation arise from the four-quark matrix elements of the potential-type operators [35] and from time-ordered products of operators describing interactions with soft gluons. The latter account, for example, for the radiative corrections to the Coulomb potential, and include the dependence of the Schrödinger potentials on logarithms of soft momenta. Adding these contributions, the effective order $1/v$ Coulomb potential is

$$\begin{aligned} \tilde{V}_c(\mathbf{p}, \mathbf{q}) = & \frac{\mathcal{V}_c^{(s)}(\nu)}{\mathbf{k}^2} - \frac{4\pi C_F \alpha_s(m\nu)}{\mathbf{k}^2} \left\{ \frac{\alpha_s(m\nu)}{4\pi} \left[-\beta_0 \ln\left(\frac{\mathbf{k}^2}{m^2\nu^2}\right) + a_1 \right] \right. \\ & \left. + \left(\frac{\alpha_s(\mu_s)}{4\pi}\right)^2 \left[\beta_0^2 \ln^2\left(\frac{\mathbf{k}^2}{m^2\nu^2}\right) - (2\beta_0 a_1 + \beta_1) \ln\left(\frac{\mathbf{k}^2}{m^2\nu^2}\right) + a_2 \right] \right\}, \end{aligned} \quad (11)$$

where $\mathbf{k} = \mathbf{p} - \mathbf{q}$ is the momentum transfer. The first term in Eq. (11) has a coefficient $\mathcal{V}_c^{(s)}(\nu)$ that contains the summation of NNLL logarithms coming from soft and ultrasoft gluons and was determined in Ref. [26]. The second term contains the one- and two-loop corrections to the Coulomb potential [36]. In vNRQCD they arise from time-ordered products of the lowest order operators describing the interaction of quarks with soft gluons [26]. The couplings in these interactions are simply $\alpha_s(\mu_s) = \alpha_s(m\nu)$ and evolve with the QCD β -function.

At NNLL order a virtual photon or Z boson produces top quarks in 3S_1 and 3P_1 states through the vector and axial-vector currents respectively. We can simplify the spin dependence of the subleading $1/m^2$ potentials by projecting onto the spin triplet channel. To do this we choose the scheme where traces over σ^i matrices are done in three dimensions (using $\mathbf{S}^2 = 2$ for triplet states).¹ The order v^0 and v^1 potentials are²

$$\tilde{V}_k(\mathbf{p}, \mathbf{q}) = \frac{\pi^2}{m|\mathbf{k}|} \mathcal{V}_k^{(s)}(\nu), \quad (12)$$

¹The difference between using three and d dimensional σ matrices is simply a change in renormalization scheme. A similar scheme dependence arises in chiral perturbation theory [37].

²At NNLO the potentials \tilde{V}_δ , \tilde{V}_r and \tilde{V}_k are equivalent to what was referred to as ‘‘Breit-Fermi’’ and ‘‘non-Abelian’’ potentials in some publications on the NNLO corrections (see e.g. [10–12]).

$$\begin{aligned}\tilde{V}_\delta(\mathbf{p}, \mathbf{q}) &= \frac{\mathcal{V}_2^{(s)}(\nu) + 2\mathcal{V}_s^{(s)}(\nu)}{m^2}, \\ \tilde{V}_r(\mathbf{p}, \mathbf{q}) &= \frac{(\mathbf{p}^2 + \mathbf{q}^2)}{2m^2\mathbf{k}^2} \mathcal{V}_r^{(s)}(\nu).\end{aligned}$$

In vNRQCD the potential coefficients at $\nu = 1$ are obtained with on-shell matching at the hard scale. The potentials \tilde{V}_δ and \tilde{V}_r are of order α_s and lead to terms in the cross section that are v^2 -suppressed. Their evolution therefore only needs to be taken into account in LL order and was determined in Ref. [23]. The potential \tilde{V}_k arises only at order α_s^2 and also leads to terms in the cross section that are v^2 -suppressed. Its evolution needs to be known at NLL and was determined in Ref. [25]. At NNLL order the complete sum of potential-like interactions is

$$\tilde{V}(\mathbf{p}, \mathbf{q}) = \tilde{V}_c(\mathbf{p}, \mathbf{q}) + \tilde{V}_\delta(\mathbf{p}, \mathbf{q}) + \tilde{V}_r(\mathbf{p}, \mathbf{q}) + \tilde{V}_k(\mathbf{p}, \mathbf{q}). \quad (13)$$

Explicit formulæ for the Wilson coefficients and constants in Eqs. (11) and (12) are collected in Appendix A.

B. Currents

To describe quark-antiquark production close to threshold at NNLL order we need to know the Wilson coefficient at NNLL order of the dimension three 3S_1 production current, and at LL order the dimension four 3P_1 and dimension five 3S_1 currents. The vector production current is $\mathbf{J}_\mathbf{p}^v = c_1\mathbf{O}_{\mathbf{p},1} + c_2\mathbf{O}_{\mathbf{p},2}$, where

$$\begin{aligned}\mathbf{O}_{\mathbf{p},1} &= \psi_\mathbf{p}^\dagger \boldsymbol{\sigma}(i\sigma_2) \chi_{-\mathbf{p}}^*, \\ \mathbf{O}_{\mathbf{p},2} &= \frac{1}{m^2} \psi_\mathbf{p}^\dagger \mathbf{p}^2 \boldsymbol{\sigma}(i\sigma_2) \chi_{-\mathbf{p}}^*,\end{aligned} \quad (14)$$

and the relevant axial-vector current is $\mathbf{J}_\mathbf{p}^a = c_3\mathbf{O}_{\mathbf{p},3}$, where

$$\mathbf{O}_{\mathbf{p},3} = \frac{-i}{2m} \psi_\mathbf{p}^\dagger [\boldsymbol{\sigma}, \boldsymbol{\sigma} \cdot \mathbf{p}] (i\sigma_2) \chi_{-\mathbf{p}}^*. \quad (15)$$

In Eqs. (14) and (15) \mathbf{p} is the soft-momentum index of the quarks. The corresponding annihilation currents $\mathbf{O}_{\mathbf{p},1-3}^\dagger$ are obtained by complex conjugation. In the basis of operators we are using there is an additional dimension five vector current,

$$\mathbf{O}_{\mathbf{p},4} = \frac{1}{m^2} \psi_\mathbf{p}^\dagger \left(\mathbf{p}(\boldsymbol{\sigma} \cdot \mathbf{p}) - \boldsymbol{\sigma} \frac{\mathbf{p}^2}{3} \right) (i\sigma_2) \chi_{-\mathbf{p}}^*. \quad (16)$$

However it produces a D -wave quark-antiquark pair and therefore does not contribute at NNLL order.

The matching condition at the hard scale for the Wilson coefficient $c_1(\nu = 1)$ is needed to order α_s^2 . Its value is determined from matching the two-loop result for the quark-antiquark production amplitude close to threshold in full QCD to the corresponding amplitude in vNRQCD and is given in Appendix A. Since the two-loop result for $c_1(1)$ is scheme dependent,

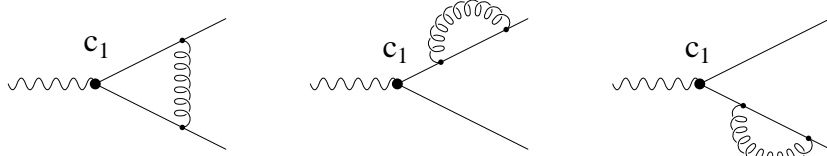


FIG. 2. Graphs with an ultrasoft gluon with $\mathbf{p} \cdot \mathbf{A}$ couplings which contribute to the running of $c_2(\nu)$.

our result is different from that obtained with the threshold expansion [32]. The LL anomalous dimension for c_1 is zero. The evolution of c_1 for $\nu < 1$ at NLL order was determined analytically in Ref. [25]. Due to the length of the resulting expression this analytic result for $\nu < 1$ is not repeated here. At NNLL order the evolution of $c_1(\nu)$ requires the three loop anomalous dimension which is not completely known. In Appendix A we discuss the form of contributions to this anomalous dimension, and investigate their effect on $c_1(\nu)$. Based on the contributions that are currently known, and a parametric estimate for the size of the unknown contributions, we find that the uncertainty in $c_1(\nu)$ from neglecting this running is likely to be at a level $\lesssim 1\%$.

The coefficients c_2 and c_3 are needed at LL order. This involves tree level matching, together with one-loop running. At tree level expanding the full theory currents, $\bar{t}\gamma t$ and $\bar{t}\gamma\gamma_5 t$ gives

$$c_2(\nu = 1) = -1/6, \quad c_3(\nu = 1) = 1. \quad (17)$$

The LL evolution of c_3 would be determined by divergent order $\alpha_s v$ graphs, but no such diagrams exist so $c_3(\nu) = 1$. For $c_2(\nu)$ we need the divergent order $\alpha_s v^2$ graphs which are shown in Fig. 2. Together they give the anomalous dimension

$$\nu \frac{\partial}{\partial \nu} c_2(\nu) = \frac{8C_F}{3\pi} \alpha_s(m\nu^2) c_1(\nu). \quad (18)$$

Integrating Eq. (18) with the boundary condition in Eq. (17) and the LL value of $c_1(\nu)$ gives the LL solution for $c_2(\nu)$:³

$$c_2(\nu) = -\frac{1}{6} - \frac{8C_F}{3\beta_0} \ln \left[\frac{\alpha_s(m\nu^2)}{\alpha_s(m)} \right]. \quad (19)$$

A check of this result is obtained by expanding in $\alpha_s(m)$

$$c_2(\nu) = -\frac{1}{6} + \frac{4C_F}{3\pi} \alpha_s(m) \ln \left(\frac{m\nu^2}{m} \right) + \dots, \quad (20)$$

where the $\ln(\nu^2)$ term agrees with the $\ln(\mu/m)$ term derived in Ref. [38]. (Note that the operator $\mathbf{O}_{p,2}$ in Ref. [38] was defined with the opposite sign.)

³ Eq. (19) was used in Ref. [21], but corrects a typo in Eq. (13) of this reference.

C. Width and Nonperturbative Effects

To incorporate the effect of the large top quark width we include in the effective Lagrangian the operators

$$\mathcal{L} = \sum_{\mathbf{p}} \psi_{\mathbf{p}}^{\dagger} \frac{i}{2} \Gamma_t \psi_{\mathbf{p}} + \sum_{\mathbf{p}} \chi_{\mathbf{p}}^{\dagger} \frac{i}{2} \Gamma_t \chi_{\mathbf{p}}. \quad (21)$$

In the Standard Model the dominant decay channel is $t \rightarrow bW^+$ and gives a width of $\Gamma_t = 1.43 \text{ GeV}$ (including one-loop electroweak [39] and two-loop QCD [40] effects). For power counting we will treat Γ_t as a fixed number to be determined from experiment. The typical energy of a Coulombic top quark is $E \sim mv^2 \sim 4 \text{ GeV}$, and we take $\Gamma_t \sim E$. Thus, the propagator for a single top (or antitop) with momentum (p^0, \mathbf{p}) is

$$\frac{i}{p^0 - \mathbf{p}^2/(2m) + i\Gamma_t/2 + i\epsilon}. \quad (22)$$

In our results the use of this propagator is equivalent to the replacement $E \rightarrow E + i\Gamma_t$ in $t\bar{t}$ Green functions from the stable quark calculation. For the total $t\bar{t}$ cross section in the Coulombic regime the operator in Eq. (21) is sufficient to account for all electroweak effects at LO [2] and NLO [30]. The complete set of electroweak effects at NNLL order is currently unknown.

The large top quark width plays a crucial role in suppressing the size of nonperturbative hadronic contributions governed by the scale Λ_{QCD} . Even at threshold ($E = 0$), the $t\bar{t}$ system has an effective energy set by the perturbative scale Γ_t . For stable quarks, an operator product expansion [41, 42] in powers of Λ_{QCD}/E can be used to incorporate non-perturbative contributions. Naively, the size of the first non-perturbative correction for $t\bar{t}$ production is therefore $[\Lambda_{\text{QCD}}/(E + i\Gamma_t)]^4$ from the gluon condensate operator. However, because the momenta of the gluons, of order Λ_{QCD} , is much smaller than the momenta of the quarks $mv \sim 25 \text{ GeV}$, their coupling to quarks is governed by a multipole expansion. The lowest order interaction is $[\psi_{\mathbf{p}}^{\dagger} \mathbf{p} \cdot \mathbf{A} \psi_{\mathbf{p}}]$, giving an additional v^2 suppression [43]. The size of the leading nonperturbative effect is therefore $\delta R^{np}/R \sim \Lambda_{\text{QCD}}^4 v^2 / (E + i\Gamma_t)^4 \lesssim 10^{-4}$. This is consistent with the size of the gluon condensate corrections to R computed in Ref. [44], and is more than two orders of magnitude smaller than the corrections considered here.

IV. TOTAL CROSS SECTION

In this section we compute the time ordered products of currents at a scale corresponding to the typical momentum and energy of the non-relativistic quarks, namely $\nu \simeq 0.15 - 0.20$. In full QCD the expression for the total cross section $\sigma_{\text{tot}}^{\gamma, Z}(e^+e^- \rightarrow \gamma^*, Z^* \rightarrow q\bar{q})$ for quarks at center of mass energy \sqrt{s} is

$$\sigma_{\text{tot}}^{\gamma, Z}(s) = \sigma_{\text{pt}} \left[F^v(s) R^v(s) + F^a(s) R^a(s) \right], \quad (23)$$

where $\sigma_{\text{pt}} = 4\pi\alpha^2/(3s)$. The vector and axial-vector R -ratios are

$$\begin{aligned}
R^v(s) &= \frac{4\pi}{s} \text{Im} \left[-i \int d^4x e^{iq \cdot x} \langle 0 | T j_\mu^v(x) j^{v\mu}(0) | 0 \rangle \right], \\
R^a(s) &= \frac{4\pi}{s} \text{Im} \left[-i \int d^4x e^{iq \cdot x} \langle 0 | T j_\mu^a(x) j^{a\mu}(0) | 0 \rangle \right],
\end{aligned} \tag{24}$$

where $q = (\sqrt{s}, 0)$ and j_μ^v (j_μ^a) is the vector (axial-vector) current that produces a quark-antiquark pair. With both γ and Z exchange the prefactors in Eq. (23) are

$$F^v(s) = \left[Q_q^2 - \frac{2s v_e v_q Q_q}{s - m_Z^2} + \frac{s^2 (v_e^2 + a_e^2) v_q^2}{(s - m_Z^2)^2} \right], \quad F^a(s) = \frac{s^2 (v_e^2 + a_e^2) a_q^2}{(s - m_Z^2)^2}, \tag{25}$$

where

$$v_f = \frac{T_3^f - 2Q_f \sin^2 \theta_W}{2 \sin \theta_W \cos \theta_W}, \quad a_f = \frac{T_3^f}{2 \sin \theta_W \cos \theta_W}. \tag{26}$$

Here Q_f is the charge for fermion f , T_3^f is the third component of weak isospin, and θ_W is the weak mixing angle.

In vNRQCD at NNLL order the current correlators are replaced by the correlators of the non-relativistic currents $\mathbf{O}_{\mathbf{p},i}$, so that

$$R^v(s) = \frac{4\pi}{s} \text{Im} \left[c_1^2(\nu) \mathcal{A}_1(v, m, \nu) + 2 c_1(\nu) c_2(\nu) \mathcal{A}_2(v, m, \nu) \right], \tag{27}$$

$$R^a(s) = \frac{4\pi}{s} \text{Im} \left[c_3^2(\nu) \mathcal{A}_3(v, m, \nu) \right], \tag{28}$$

with

$$\begin{aligned}
\mathcal{A}_1(v, m, \nu) &= i \sum_{\mathbf{p}, \mathbf{p}'} \int d^4x e^{i\hat{q} \cdot x} \langle 0 | T \mathbf{O}_{\mathbf{p},1}(x) \mathbf{O}_{\mathbf{p}',1}^\dagger(0) | 0 \rangle, \\
\mathcal{A}_2(v, m, \nu) &= \frac{i}{2} \sum_{\mathbf{p}, \mathbf{p}'} \int d^4x e^{i\hat{q} \cdot x} \langle 0 | T \left[\mathbf{O}_{\mathbf{p},1}(x) \mathbf{O}_{\mathbf{p}',2}^\dagger(0) + \mathbf{O}_{\mathbf{p},2}(x) \mathbf{O}_{\mathbf{p}',1}^\dagger(0) \right] | 0 \rangle, \\
\mathcal{A}_3(v, m, \nu) &= i \sum_{\mathbf{p}, \mathbf{p}'} \int d^4x e^{i\hat{q} \cdot x} \langle 0 | T \mathbf{O}_{\mathbf{p},3}(x) \mathbf{O}_{\mathbf{p}',3}^\dagger(0) | 0 \rangle.
\end{aligned} \tag{29}$$

Here $\hat{q} \equiv (\sqrt{s} - 2m, 0)$, and the current operators $\mathbf{O}_{\mathbf{p},i}$ are defined in Eqs. (14) and (15). The correlators \mathcal{A}_i are functions of the quark mass m , velocity renormalization scale ν , and the effective velocity

$$v = \left(\frac{\sqrt{s} - 2m + i\Gamma_t}{m} \right)^{\frac{1}{2}}. \tag{30}$$

Here m is the pole mass. For our calculation evaluating matrix elements at the low-scale corresponds to computing the \mathcal{A}_i 's with ν of the order a typical Coulombic top quark's velocity. The correlator \mathcal{A}_2 can be related to \mathcal{A}_1 using the quark equation of motion giving

$$\mathcal{A}_2(v, m, \nu) = v^2 \mathcal{A}_1(v, m, \nu). \tag{31}$$

Performing the spin traces in 3-dimensions the correlators \mathcal{A}_1 and \mathcal{A}_3 are determined by the zero-distance coordinate space Green functions,

$$\begin{aligned}\mathcal{A}_1(v, m, \nu) &= 6 N_c \mu_S^{4\epsilon} \int D^n \mathbf{p} D^n \mathbf{p}' \tilde{G}_{v,m,\nu}(\mathbf{p}, \mathbf{p}'), \\ \mathcal{A}_3(v, m, \nu) &= \frac{12 N_c}{m^2 n} \mu_S^{4\epsilon} \int D^n \mathbf{p} D^n \mathbf{p}' (\mathbf{p} \cdot \mathbf{p}') \tilde{G}_{v,m,\nu}(\mathbf{p}, \mathbf{p}').\end{aligned}\quad (32)$$

Here $n \equiv d-1 = 3-2\epsilon$, we use $D^n \mathbf{k} \equiv e^{\epsilon\gamma_E} (4\pi)^{-\epsilon} d^n \mathbf{k} / (2\pi)^n$ which converts μ_S (and ν) from the MS to the $\overline{\text{MS}}$ scheme, and $N_c = 3$ is the number of colors. The dependence of the \mathcal{A}_3 prefactor on n comes from taking the trace over $\boldsymbol{\sigma}$ matrices in the P -wave current in 3 dimensions, and then projecting the dot product $\mathbf{p} \cdot \mathbf{p}'$ back into n -dimensions.

To determine the correlators \mathcal{A}_1 and \mathcal{A}_3 at NNLL order we use a combination of numerical and analytic calculations. Ultraviolet divergent contributions are computed with dimensional regularization in the $\overline{\text{MS}}$ scheme, which is required for consistency with the scheme used to compute the matching and running of the Wilson coefficients. Our strategy for the analytic calculations for these potentials follows that in Ref. [10]. In momentum space the NNLL Schrödinger equation for the Green function for a color singlet quark-antiquark pair is

$$\left[\frac{\mathbf{p}^2}{m} - \frac{\mathbf{p}^4}{4m^3} - \tilde{E} \right] \tilde{G}_{s,m,\nu}(\mathbf{p}, \mathbf{p}') + \int D^n \mathbf{k} \mu_S^{2\epsilon} \tilde{V}(\mathbf{p}, \mathbf{k}) \tilde{G}_{s,m,\nu}(\mathbf{k}, \mathbf{p}') = (2\pi)^n \delta^{(n)}(\mathbf{p} - \mathbf{p}'), \quad (33)$$

where $\tilde{E} \equiv mv^2$ and $\tilde{V}(\mathbf{p}, \mathbf{k})$ is given in Eq. (13).

We start with the vector correlator \mathcal{A}_1 . The lowest order S -wave Coulomb Green function at zero distances reads

$$\begin{aligned}G^0(a, v, m, \nu) &= \frac{m^2}{4\pi} \left\{ i v - a \left[\ln \left(\frac{-i v}{\nu} \right) - \frac{1}{2} + \ln 2 + \gamma_E + \psi \left(1 - \frac{i a}{2 v} \right) \right] \right\} \\ &\quad + \frac{m^2 a}{4\pi} \frac{1}{4\epsilon}\end{aligned}\quad (34)$$

where $a \equiv -\mathcal{V}_c(\nu)/(4\pi)$. Eq. (34) is a standard result [45], except for the scheme dependent constants entering with the divergence. This term was computed from the two-loop graph with a single \mathcal{V}_c insertion, and Eq. (34) agrees with the $\overline{\text{MS}}$ result obtained in Ref. [46]. The $1/\epsilon$ pole is canceled by a counterterm for the time ordered product of currents. An identical divergence structure appears with the full \tilde{V}_c potential in Eq. (11). Since this divergence and corresponding constants appear only in the real part of G^0 , for the purpose of computing $\text{Im}[\mathcal{A}_1]$ it does not matter whether or not they are subtracted in $\overline{\text{MS}}$. Therefore, we determine the contribution from the Coulomb potential by the exact solution of the equation

$$\left[\frac{\mathbf{p}^2}{m} - E \right] \tilde{G}_{v,m,\nu}^c(\mathbf{p}, \mathbf{p}') + \int \frac{d^3 \mathbf{k}}{(2\pi)^3} \tilde{V}_c(\mathbf{p}, \mathbf{k}) \tilde{G}_{v,m,\nu}^c(\mathbf{k}, \mathbf{p}') = (2\pi)^3 \delta^{(3)}(\mathbf{p} - \mathbf{p}'), \quad (35)$$

using numerical techniques developed in Refs. [3,4]. We will denote by $G^c(a, v, m, \nu)$ the solution for the zero-distance coordinate space Green function obtained from $\tilde{G}^c(v, m, \nu)(\mathbf{p}, \mathbf{p}')$.

On the other hand, the first order perturbative corrections to $\mathcal{A}_1(v, m, \nu)$ from the potentials \tilde{V}_k , \tilde{V}_δ , and \tilde{V}_r , and the kinetic energy correction, $\mathbf{p}^4/(4m^3)$, have ultraviolet subdivergences which must be subtracted in $\overline{\text{MS}}$. For the first order corrections to the zero-distance Green function in dimensional regularization from the kinetic energy correction and the potentials \tilde{V}_k , \tilde{V}_δ , \tilde{V}_r (leaving out the Wilson coefficients) we find:

$$\begin{aligned} \delta G^{\text{kin}}(a, v, m, \nu) &= \frac{a m^2}{16\pi} \left\{ i v - a \left[\ln \left(\frac{-i v}{\nu} \right) - \frac{3}{2} + \ln 2 + \gamma_E + \psi \left(1 - \frac{i a}{2 v} \right) \right] \right\}^2 \\ &\quad - \frac{m^2}{16\pi} \left[-a v^2 + \frac{a^3}{4} \left(\frac{1}{4\epsilon^2} - \frac{1}{\epsilon} - 2 \right) \right] \\ &\quad + \frac{v^2}{2} \left(1 + a \frac{\partial}{\partial a} + \frac{v}{4} \frac{\partial}{\partial v} \right) G^0(a, v, m, \nu), \end{aligned} \quad (36)$$

$$\begin{aligned} \delta G^k(a, v, m, \nu) &= -\frac{m^2}{8\pi a} \left\{ i v - a \left[\ln \left(\frac{-i v}{\nu} \right) - 2 + 2 \ln 2 + \gamma_E + \psi \left(1 - \frac{i a}{2 v} \right) \right] \right\}^2 \\ &\quad + \frac{m^2}{8\pi a} \left[-v^2 + \frac{a^2}{4} \left(\frac{1}{3\epsilon^2} - \frac{2}{\epsilon} \left(1 - \frac{2}{3} \ln 2 \right) + \frac{4}{3} - 8 \ln 2 + \frac{8}{3} \ln^2 2 + \frac{\pi^2}{9} \right) \right], \end{aligned} \quad (37)$$

$$\begin{aligned} \delta G^\delta(a, v, m, \nu) &= -\frac{m^2}{16\pi^2} \left\{ i v - a \left[\ln \left(\frac{-i v}{\nu} \right) - \frac{1}{2} + \ln 2 + \gamma_E + \psi \left(1 - \frac{i a}{2 v} \right) \right] \right\}^2 \\ &\quad + \frac{m^2 a^2}{256\pi^2} \frac{1}{\epsilon}, \end{aligned} \quad (38)$$

$$\begin{aligned} \delta G^r(a, v, m, \nu) &= -\frac{m^2}{16\pi^2} \left\{ i v - a \left[\ln \left(\frac{-i v}{\nu} \right) - \frac{3}{2} + \ln 2 + \gamma_E + \psi \left(1 - \frac{i a}{2 v} \right) \right] \right\}^2 \\ &\quad + \frac{m^2}{16\pi^2} \left[-v^2 + \frac{a^2}{4} \left(\frac{1}{4\epsilon^2} - \frac{1}{\epsilon} - 2 \right) \right] - \frac{v^2}{4\pi} \frac{\partial}{\partial a} G^0(a, v, m, \nu). \end{aligned} \quad (39)$$

In deriving these equations we have included the counterterms generated by renormalizing the $\mathbf{O}_{p,1}$ current [22] at NLL order. These counterterm graphs are sufficient to cancel all subdivergences. The remaining overall divergences in Eqs. (36) to (39) are of the form $1/\epsilon$ and v^2/ϵ and are canceled by vacuum counterterms for the current correlator, and can be dropped. The final renormalized expression for the NNLL vector correlator \mathcal{A}_1 is then

$$\begin{aligned} \mathcal{A}_1(v, m, \nu) &= 6 N_c \left[G^c(a, v, m, \nu) + \left(\mathcal{V}_2^{(s)}(\nu) + 2\mathcal{V}_s^{(s)}(\nu) \right) \delta G^\delta(a, v, m, \nu) \right. \\ &\quad \left. + \mathcal{V}_r^{(s)}(\nu) \delta G^r(a, v, m, \nu) + \mathcal{V}_k^{(s)}(\nu) \delta G^k(a, v, m, \nu) + \delta G^{\text{kin}}(a, v, m, \nu) \right]. \end{aligned} \quad (40)$$

For the computation of the axial-vector correlator \mathcal{A}_3 at NNLL we only need to consider the leading order Green function because the axial-vector current is already suppressed by one power of the velocity. As \mathcal{A}_3 describes P -wave quark-antiquark production it is proportional to the $l = 1$ component of the Coulomb Green function at zero distance,

$$\begin{aligned} G^1(a, v, m, \nu) &= \frac{m^4}{4\pi} \left\{ i v^3 - a v^2 \left[\ln \left(\frac{-i v}{\nu} \right) - 1 + \ln 2 + \gamma_E + \Psi \left(1 - \frac{i a}{2 v} \right) \right] \right. \\ &\quad \left. + i \frac{v a^2}{4} - \frac{a^3}{4} \left[\ln \left(\frac{-i v}{\nu} \right) - \frac{7}{4} + \ln 2 + \gamma_E + \Psi \left(1 - \frac{i a}{2 v} \right) \right] \right\} \\ &\quad + \frac{m^4}{16\pi} \left(\frac{1}{\epsilon} + \frac{2}{3} \right) \left(v^2 a + \frac{a^3}{8} \right). \end{aligned} \quad (41)$$

The divergences and constants were determined by explicitly computing the two-loop and four-loop potential graphs in the $\overline{\text{MS}}$ scheme (with one and three \mathcal{V}_c insertions respectively).

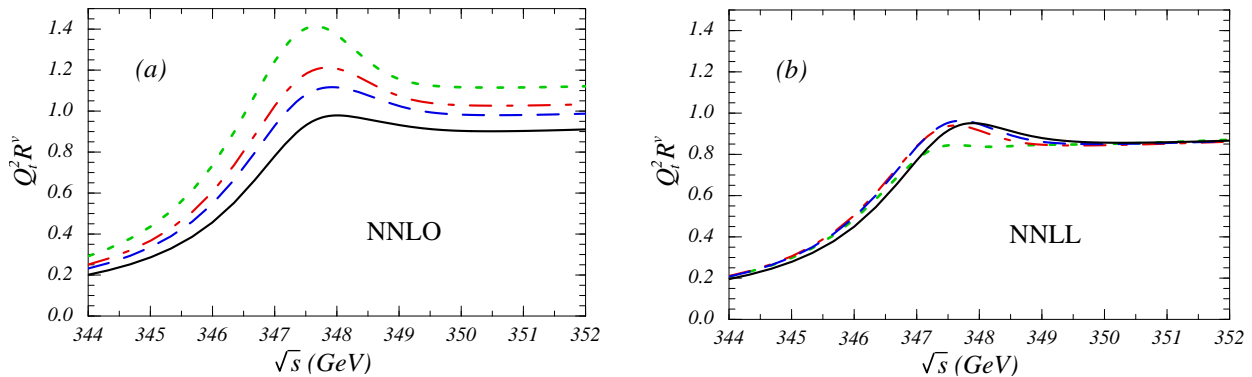


FIG. 3. Results for the vector current R -ratio in Eq. (27) with a fixed pole mass, $m_t = 175$ GeV. In (a) we reproduce the NNLO pole mass results (with matching values for Wilson coefficients). In (b) we display our NNLL pole mass results (with running coefficients). In both plots the dotted, dot-dashed, dashed, and solid curves correspond to $\nu = 0.1, 0.15, 0.2$, and 0.4 respectively.

As before, the result contains overall divergences of the form $1/\epsilon$ and v^2/ϵ that are canceled by vacuum counterterms. The final result for the axial-vector correlator \mathcal{A}_3 is

$$\mathcal{A}_3(v, m, \nu) = \frac{4 N_c}{m^2} G^1(a, v, m, \nu). \quad (42)$$

The (fixed order) NLO and NNLO corrections to \mathcal{A}_3 are known [16,47]. Since they contribute to $\sigma_{\text{tot}}^{\gamma, Z}$ beyond NNLL order, they are not included in our analysis.

We emphasize again that the use of Eq. (30) in determining $R^{v,a}$ does not provide a consistent treatment of the top quark width at NNLL order. This can be seen from the presence of ν -dependent terms proportional to $\alpha_s \Gamma_t / m_t \ln(\nu/a)$ in the imaginary part of Eq. (40) [10], and from a scheme dependent term proportional to $\alpha_s \Gamma_t / m_t$ in the imaginary part of Eq. (41). These terms are energy independent and parametrically of NNLL order. Conceptually, they indicate that additional renormalization and matching is necessary to achieve a consistent treatment of all electroweak effects at this order. The issue of electroweak effects in the total cross section will be addressed elsewhere.

V. POLE MASS RESULTS

Let us briefly examine the results for R^v and R^a in the pole mass scheme. In Fig. 3a the NNLO photon-induced cross section $Q_t^2 R^v$ is displayed over the c.m. energy \sqrt{s} for $\alpha_s(m_Z) = 0.118$, pole mass $m_t = 175$ GeV, $\Gamma_t = 1.43$ GeV, and for $\nu = 0.1, 0.15, 0.2$ and 0.4 . For the strong coupling four-loop running is employed and all light quark flavors ($n_f = 5$) are taken massless. Following Ref. [17] we have defined NNLO by taking $\nu = 1$ in the current Wilson coefficients $c_{1,2}(\nu)$ and in the $\ln(-iv/\nu)$ terms in the Green functions $\delta G^{\text{kin}, k, \delta, r}$. A lower scale $\mu_{\text{soft}} = m_t \nu$ is used for factors of α_s that appear in both the Green functions and in $\mathcal{V}_i(\nu = 1)$. At NNLO the size of the corrections and the dependence on ν are found to be similar to previous NNLO calculations [17], indicating that our calculational strategy does not change the fixed order results.

In Fig. 3b we show the renormalization group improved NNLL pole mass results for the same parameters and range of ν used in Fig. 3a. From the physical point of view the appropriate choice of the subtraction velocity parameter ν is around $C_F\alpha_s \approx 0.15$ – 0.2 . With this choice all large logarithms of ratios of the the hard and the non-relativistic scales are summed in the Wilson coefficients, and the matrix elements of vNRQCD operators are free of large logarithmic terms. To be conservative we show a larger range of values, $\nu = 0.1$ – 0.4 , in Fig. 3. In both the NNLO and NNLL results the dependence of the peak location on ν is a reflection of the use of the pole mass and is considerably reduced if threshold masses are employed [17] as we do in the next section. From Fig. 3 we already see that the dependence on ν of the normalization of the NNLL results is significantly reduced in comparison to the NNLO results. This is discussed in more detail in the following section.

An issue we would like to discuss here concerns the flattening of the peak that is observed for the NNLL $\nu = 0.1$ curve in Fig. 3b. This flattening turns out to be specific to the use of the pole mass together with our calculational strategy. To see this consider the contribution from the $n = 1$, 3S_1 bound state to R^v . Up to trivial factors its contribution to the cross section based on Eq. (40) reads

$$R_{n=1}^v \propto \text{Im} \left[\frac{|\Psi_c(0)|^2}{E_c - E - i\Gamma_t} + \frac{\delta|\Psi(0)|_m^2}{E^0 - E - i\Gamma_t} - \frac{\delta E_m |\Psi^0(0)|^2}{(E^0 - E - i\Gamma_t)^2} \right]. \quad (43)$$

Here $|\Psi_c(0)|^2$ and E_c are the square of the wave function at the origin and the binding energy of the ground state obtained from Eq. (35), and $\delta|\Psi(0)|_m^2$ and δE_m are the corresponding perturbative corrections from the potentials \tilde{V}_k , \tilde{V}_δ , \tilde{V}_r and the kinetic energy correction $\mathbf{p}^4/4m^3$. The terms $|\Psi^0(0)|^2 = m_t^3 a^3/(8\pi n^3)$ and $E^0 = -m_t a^2/4$ are the LL squared wave function at the origin and binding energy, respectively. Explicit formulas for E_c and δE_m including the summation of logarithms of v have been presented in Ref. [26]. If the unexpanded NNLL Schrödinger Equation in Eq. (33) is used, then Eq. (43) becomes

$$R_{n=1}^v \propto \text{Im} \left[\frac{|\Psi_c(0)|^2 + \delta|\Psi(0)|_m^2}{E_c + \delta E_m - E - i\Gamma_t} \right]. \quad (44)$$

For $E \approx E_c$ and $\delta E_m > 30$ MeV the relative difference between Eq. (44) and (43) is of order $-\delta E_m/\Gamma_t$, because $E^0 - E_c \approx 1$ GeV is large. For $\nu = (0.1, 0.15, 0.2, 0.3, 0.4)$ and using the same parameters as in Fig 3a, we obtain $\delta E_m = (143, 27, -10, -33, -40)$ MeV. Thus for $\nu = 0.1$ our calculational method leads to negative contributions of about 10% at energies around the nominal peak position with respect to a calculational strategy which instead involves the contribution in Eq. (44). This is observed in Fig. 3b for $\nu = 0.1$. We have checked that one can cure this flattening by summing the perturbative contributions in Eq. (43) into the single energy denominator of Eq. (44) (see also [13, 16]). However, this procedure sums terms that are subleading according to the power counting.

Instead, we note that this effect would be small if $E^0 - E_c \ll 1$ GeV. Thus, it can be regarded as a direct consequence of the pole mass scheme where this energy difference is large due to an infrared renormalon. In the subsequent section we will make use of the 1S mass scheme [48], together with our calculation strategy. In this case the flattening effect does not occur because properly introducing the 1S mass makes the analogue of the third term in Eq. (43) explicitly zero.

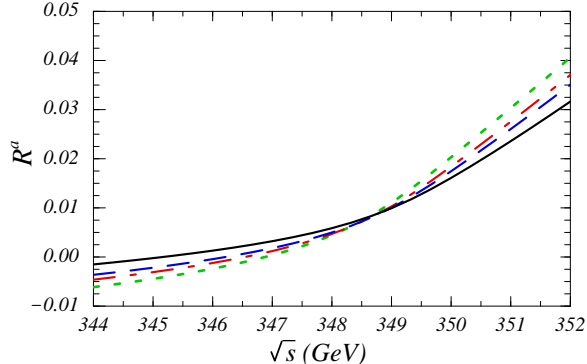


FIG. 4. Pole mass results for the axial-vector current R -ratio in Eq. (27). The dotted, dashed, dot-dashed, and solid curves correspond to $\nu = 0.1, 0.15, 0.2$, and 0.4 respectively.

In Fig. 4 the NNLL order axial-vector current induced cross section R^a is displayed over the c.m. energy \sqrt{s} for $m_t = 175$ GeV, $\alpha_s(m_Z) = 0.118$ and $\Gamma_t = 1.43$ GeV for $\nu = 0.1, 0.15, 0.2$ and 0.4 . As expected from the power counting, R^a is at the percent level and suppressed by two orders of magnitude with respect to R^v at c.m. energies close to the 1S peak and continuously grows for larger energies. No peak-like structure is visible since the P -wave wavefunctions are zero at the origin. For $\sqrt{s} \lesssim 348$ GeV it is conspicuous that R^a becomes slightly negative. This unphysical behavior of R^a arises because we have not included a complete treatment of top width effects at NNLO. In particular there are short-distance corrections which in the non-relativistic theory correct for the true physical top phase space [15]. Integration over the true top phase space, of course, leads to a positive cross section. As the difference between the approximate and true phase space integration involves only hard momenta, it corresponds to a short-distance correction. We note that unlike $\overline{\text{MS}}$, in a hard cutoff scheme the cross section remains positive [15] because there is no way to generate a negative result by cutting off the integration region of a squared matrix element. In any case, like other known subleading width effects these corrections are quite small, of order $\Gamma_t/m_t \sim 0.01$ for both R^v and R^a [15].

VI. THE 1S TOP QUARK MASS

Although the heavy quark pole mass is IR-finite [49, 50] and convenient to use in bound state calculations, it suffers from a linear sensitivity to small momenta, which leads to an ambiguity of order Λ_{QCD} associated to the notion of the pole mass [51]. In practical bound state calculations based on the Schrödinger equation this ambiguity turns up as large r -independent perturbative corrections in the coordinate space Coulomb potential $V_c(r)$. These corrections grow asymptotically like $-\mu_S \alpha_s^n n!$ [52]. Because the top quark mass can be determined from the threshold scan at a future lepton collider with experimental uncertainties smaller than Λ_{QCD} [18], it is advantageous to abandon the pole mass definition and replace it with a so-called “threshold mass”.

Threshold masses are short-distance mass definitions, i.e. their ambiguity is parametrically smaller than Λ_{QCD} , and the expansion relating them to the $\overline{\text{MS}}$ mass converges very

well. They remove the large perturbative corrections in a systematic way order by order in perturbation theory based on the fact that the total static energy $E_{\text{stat}} = 2m_t + V_c(r)$ is free of an ambiguity of order Λ_{QCD} [53, 54]. At the same time, threshold masses differ from the pole mass by corrections that are parametrically of order $m\alpha_s^2$ and comply with the non-relativistic power-counting [54] (see Eq. (33), where all leading order terms are of order $m\alpha_s^2$). In other words, threshold masses account for the fact that the quark is off-shell only by a small amount of the order $v^2 \sim \alpha_s^2 \ll 1$. In this work we use the 1S top quark mass definition [15], which is defined as half of the mass of a perturbative contribution to the fictitious stable 3S_1 toponium ground state. In recent NNLO calculations of the threshold cross section alternative threshold mass definitions have also been used such as the “kinetic mass” [55], and the “potential subtracted mass” [54] and variants of it [56]. (See Ref. [17] for a comparison of threshold mass definitions.)

The relation between the 1S mass and the pole mass can be obtained from the 3S_1 ground state ($n = 1$) solution of Eq. (33) and reads,

$$M_t^{\text{1S}} = m_t \left\{ 1 - [\Delta^{\text{LL}}] - [\Delta^{\text{NLL}}] - [\Delta_c^{\text{NNLL}} + \Delta_m^{\text{NNLL}}] \right\}, \quad (45)$$

where [recalling that $a \equiv -\mathcal{V}_c^{(s)}(\nu)/(4\pi)$]

$$\begin{aligned} \Delta^{\text{LL}}(\nu) &= \frac{a^2}{8}, \\ \Delta^{\text{NLL}}(\nu) &= \frac{a^3}{8\pi C_F} \left[\beta_0 \left(L + 1 \right) + \frac{a_1}{2} \right], \\ \Delta_c^{\text{NNLL}}(\nu) &= \frac{a^4}{8\pi^2 C_F^2} \left[\beta_0^2 \left(\frac{3}{4}L^2 + L + \frac{\zeta_3}{2} + \frac{\pi^2}{24} + \frac{1}{4} \right) + \beta_0 \frac{a_1}{2} \left(\frac{3}{2}L + 1 \right) \right. \\ &\quad \left. + \frac{\beta_1}{4} \left(L + 1 \right) + \frac{a_1^2}{16} + \frac{a_2}{8} \right], \\ \Delta_m^{\text{NNLL}}(\nu) &= -\frac{a^2}{8} \mathcal{V}_k^{(s)}(\nu) - \frac{a^3}{8\pi} \left[\frac{\mathcal{V}_2^{(s)}(\nu)}{2} + \mathcal{V}_s^{(s)}(\nu) + \frac{3\mathcal{V}_r^{(s)}(\nu)}{8} \right] + \frac{5}{128} a^4, \\ L &\equiv \ln \left(\frac{\nu}{a} \right). \end{aligned} \quad (46)$$

For convenience, we have displayed the LL, NLL and NNLL contributions separately. The term Δ_c^{NNLL} denotes the NNLL corrections from the Coulomb potential \tilde{V}_c , and Δ_m^{NNLL} the ones from the potentials \tilde{V}_δ , \tilde{V}_r and \tilde{V}_k and from the kinetic energy correction $\mathbf{p}^4/4m^3$. For Δ^{NLL} and $\Delta_{c,m}^{\text{NNLL}}$ the difference between using a and $C_F \alpha_s(M_t^{\text{1S}}\nu)$ only enters beyond NNLL. Using the non-relativistic power-counting, which is required to correctly eliminate the pole mass, the inverse of Eq. (45) reads,

$$m_t = M_t^{\text{1S}} \left\{ 1 + [\Delta^{\text{LL}}] + [\Delta^{\text{NLL}}] + [(\Delta^{\text{LL}})^2 + \Delta_c^{\text{NNLL}} + \Delta_m^{\text{NNLL}}] \right\}, \quad (47)$$

where the LL, NLL and NNLL corrections are each given in brackets. It is mandatory to use relation (47) at LL, NLL and NNLL for the LL, NLL and NNLL cross section at the same low-scale subtraction velocity ν in order to guarantee the proper cancellation of the large corrections associated with the pole mass ambiguity.

In all of the Wilson coefficients for the potentials and currents the replacement $m_t \rightarrow M_t^{1S}$ suffices at NNLL order. This is because m_t and M_t^{1S} differ by an order v^2 amount. Expanding the small logarithm, $\ln(1 + \Delta_{LL})$, gives

$$\alpha_s(m_t) = \alpha_s(M_t^{1S}) - \frac{\beta_0}{2\pi} \alpha_s^2(M_t^{1S}) \Delta_{LL} + \dots \quad (48)$$

The expansions for $\alpha_s(m_t\nu)$ and $\alpha_s(m_t\nu^2)$ in terms of $\alpha_s(M_t^{1S}\nu)$ and $\alpha_s(M_t^{1S}\nu^2)$ are analogous. Since $\Delta_{LL} \sim v^2$ the second term in Eq. (48) gives a v^3 correction, and in the cross section enters at N³LL (or higher).

Implementing the replacement in Eq. (47) in the low energy Green functions is more involved. We implement the additional corrections in the Schrödinger equation in Eq. (33) following the calculational strategy used in Sec. IV. The corrections in Eq. (47) that arise from the Coulomb potential, Δ_{LL} , Δ_{NLL} and Δ_c^{NNLL} , are implemented through Eq. (35), which we solve exactly. This accounts for the corrections arising from the definition of the energy $E = \sqrt{s} - 2m_t$ and the corrections coming from the leading \mathbf{p}^2/m_t kinetic energy term. (For the latter only the LL correction Δ_{LL} is needed.) The term Δ_m^{NNLL} from the energy definition is treated perturbatively and leads to an additional correction to the correlator \mathcal{A}_1 that reads,

$$\begin{aligned} \delta\mathcal{A}_1(v, M_t^{1S}, \nu) &= 6 N_c \delta G^{1S}(a, v, M_t^{1S}, \nu), \\ \delta G^{1S}(a, v, M_t^{1S}, \nu) &= -\frac{\Delta_m^{NNLL}}{v} \frac{d}{dv} G^0(a, v, M_t^{1S}, \nu). \end{aligned} \quad (49)$$

δG^{1S} is an order v^2 correction since $v^{-1}d/dv \sim v^{-2}$ compensates $\Delta_m^{NNLL} \sim v^4$. Finally, in all v^2 -suppressed Green functions (Sec. IV, Eqs. (36)–(39) and $\mathcal{A}_{2,3}$), the LL correction Δ_{LL} needs to be included using

$$v = \left(\frac{\sqrt{s} - 2M_t^{1S}(1 + \Delta_{LL}) + i\Gamma_t}{M_t^{1S}} \right)^{\frac{1}{2}} \quad (50)$$

rather than Eq. (30) as the definition of the velocity, and the pole mass m_t has to be replaced by M_t^{1S} everywhere else. This procedure correctly implements the 1S mass scheme at NNLL order.

In the 1S mass scheme multiple bound state energy poles in \mathcal{A}_1 caused by the perturbative treatment of the potentials $\tilde{V}_{\delta,r,k}$ and the kinetic energy correction only exist for higher radial excitations ($n \geq 2$), but not for the ground state ($n = 1$) that is responsible for the 1S peak visible in the lineshape. This can be seen from Eq. (49), which exactly cancels the ground state double pole terms from Eqs. (36)–(39). The corrections that arise from removing the double pole terms for $n \geq 2$ by summing the Δ_m^{NNLL} energy shifts into single energy denominators are found to be at the per-mille level and negligible.

In non-threshold processes the $\overline{\text{MS}}$ top quark mass is typically a more convenient mass definition to use than a threshold mass. The 1S mass is a scale-independent quantity, and its relation to the $\overline{\text{MS}}$ mass can be determined using the epsilon expansion [48] at $\mu = m_t$ ($\nu = 1$). Explicit formulæ for the determination of the top $\overline{\text{MS}}$ mass from the top 1S mass can be found in Ref. [57].

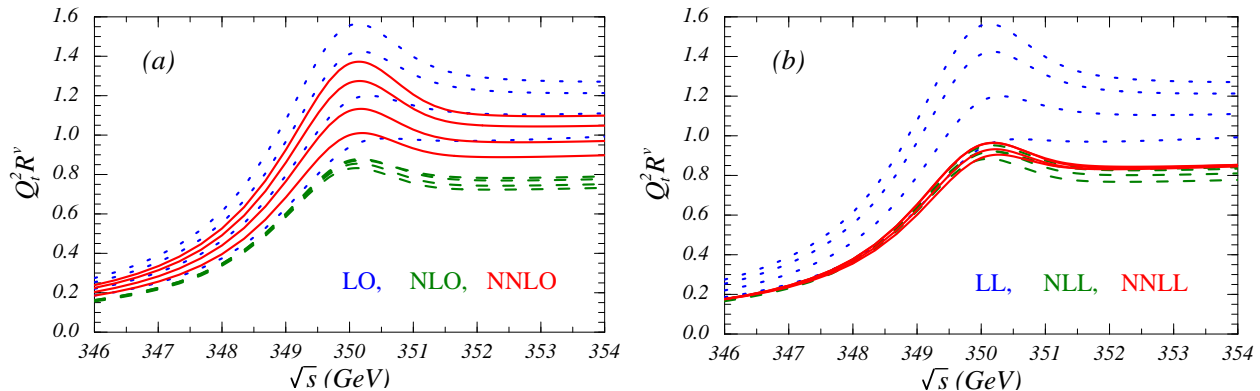


FIG. 5. Comparison of $Q_t^2 R^{\nu}$ with fixed M_t^{1S} mass for the fixed order and resummed expansions. The dotted, dashed, and solid curves in a) are LO, NLO, and NNLO, and in b) are LL, NLL, and NNLL order. For each order four curves are plotted for $\nu = 0.1, 0.125, 0.2, \text{ and } 0.4$.

\sqrt{s} (GeV)		347	350	353
$Q_t^2 R_{LL}^{\nu}$	$\nu = 0.1$	0.387	1.556	1.276
	$\nu = 0.125$	0.355	1.411	1.215
	$\nu = 0.2$	0.302	1.175	1.105
	$\nu = 0.275$	0.276	1.054	1.043
	$\nu = 0.4$	0.251	0.940	0.980
$Q_t^2 R_{NLL}^{\nu}$	$\nu = 0.1$	0.230	0.881	0.770
	$\nu = 0.125$	0.237	0.917	0.804
	$\nu = 0.2$	0.243	0.944	0.835
	$\nu = 0.275$	0.242	0.937	0.837
	$\nu = 0.4$	0.237	0.912	0.827
$Q_t^2 R_{NNLL}^{\nu}$	$\nu = 0.1$	0.237	0.888	0.842
	$\nu = 0.125$	0.240	0.920	0.836
	$\nu = 0.2$	0.244	0.955	0.841
	$\nu = 0.275$	0.245	0.961	0.845
	$\nu = 0.4$	0.244	0.955	0.846

TABLE I. Numerical values of $Q_t^2 R^{\nu}$ which appear in the NNLL results in Fig. 5b.

VII. DISCUSSION

In this section we carry out a detailed analysis of R^{ν} and R^a in the 1S mass scheme with the main emphasis on assessing the remaining theoretical uncertainties in our computation. In Fig. 5 we have displayed results for $Q_t^2 R^{\nu}$ over the c.m. energy \sqrt{s} for $M_t^{1S} = 175$ GeV, $\alpha_s(m_Z) = 0.118$ and $\Gamma_t = 1.43$ GeV. For the strong coupling four-loop running is employed and all light quark flavors ($n_f = 5$) are taken massless. Fig. 5a shows results at LO (dotted blue lines), NLO (dashed green lines) and NNLO (solid red lines), while Fig. 5b shows the

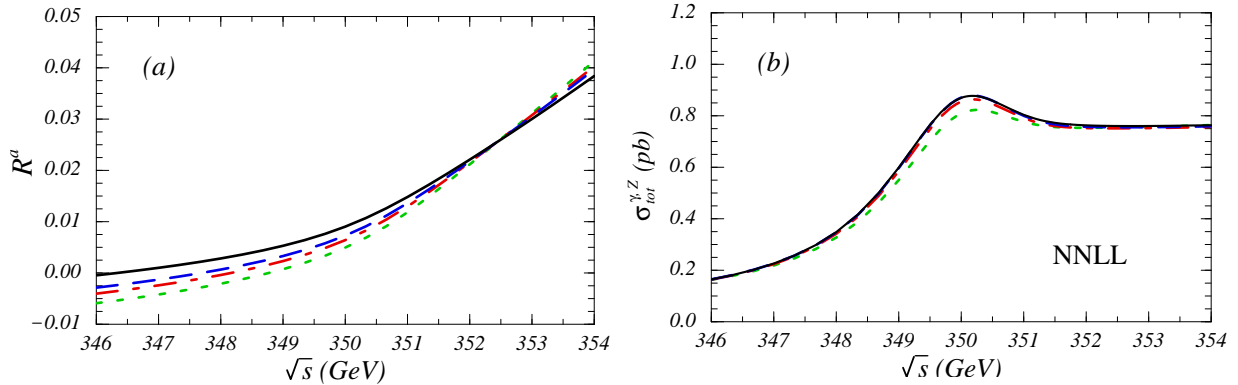


FIG. 6. Using the M_t^{1S} mass a) shows the LL result for R^a , and b) shows the total NNLL cross section in pb . The dotted, dashed, dot-dashed, and solid curves correspond to $\nu = 0.1, 0.15, 0.2,$ and 0.4 .

resummed results at LL (dotted blue lines), NLL (dashed green lines) and NNLL (solid red lines) order. At each order four curves are displayed corresponding to $\nu = 0.1, 0.125, 0.2,$ and 0.4 . At $\sqrt{s} = 350$ GeV the LO, LL, and NNLO upper through lower lines correspond monotonically to $\nu = 0.1$ through $\nu = 0.4$. In contrast, the upper through lower NLO lines correspond to $\nu = 0.4$ through $\nu = 0.1$. At NLL the lower and upper lines at $\sqrt{s} = 350$ GeV correspond to $\nu = 0.1$ and $\nu = 0.2$ (whereas $\nu = 0.4$ lies in between). Finally, at NNLL the lower line is $\nu = 0.1$, while the upper line includes both $\nu = 0.2$ and $\nu = 0.4$ at the displayed resolution. Our NNLO results agree well with previous NNLO analyses, see Ref. [17] for a synopsis of previous NNLO results. In Table I we have summarized the NNLL values for $Q_t^2 R^v$ for $\sqrt{s} = 347, 350$ and 353 GeV with the same parameters as used in the figure. The values $\nu = 0.125$ and $\nu = 0.275$ are included in the Table since at $\sqrt{s} = 353$ the value of $Q_t^2 R^v$ is minimized near $\nu = 0.125$, while for $\sqrt{s} = 350$ its value is maximized near $\nu = 0.275$.

For R^v the LL cross section is equivalent to the LO one because the one-loop anomalous dimension of c_1 vanishes. The NLL cross section is obtained by eliminating from Eq. (40) the corrections from the $1/m$ -suppressed potentials, the kinetic energy term ($\mathbf{p}^4/4m^3$) and the operators $\mathbf{O}_{p,2}$ and $\mathbf{O}_{p,3}$. For c_1 the NLL evolution and the one-loop matching condition is employed. For the Coulomb potential, the coupling $\mathcal{V}_c(\nu)$ is set equal to $-4\pi C_F \alpha_s(M_t^{1S}\nu)$, and only the one-loop corrections proportional to $[\alpha_s(M_t^{1S}\nu)]^2$ have to be taken into account.

In Fig. 6a we have displayed R^a at LL for $M_t^{1S} = 175$ GeV, $\alpha_s(m_Z) = 0.118$ and $\Gamma_t = 1.43$ GeV and $\nu = 0.1, 0.15, 0.2, 0.4$. The lower through upper lines for $\sqrt{s} < 352$ GeV correspond monotonically to $\nu = 0.1$ through $\nu = 0.4$. With the 1S mass, R^a dips below zero for $\sqrt{s} \lesssim 347$ GeV. This dip has the same origin as for the pole mass and is discussed in section V. Finally, in Fig. 6b we have displayed our total NNLL result for the $\gamma + Z$ induced cross section, using the same parameters as in Fig. 6a.

Comparing Figs. 5a and 5b the variation of the normalization of R^v with ν at NNLL order is considerably reduced in comparison to the NNLO result. Equally important, the size of the NNLL corrections is considerably smaller than the size of the corresponding NNLO corrections. The latter indicates that at the low scale the perturbative corrections to the threshold $t\bar{t}$ cross section are converging. In $\sigma_{\text{tot}}^{\gamma,Z}$ the remaining variation of R^v with

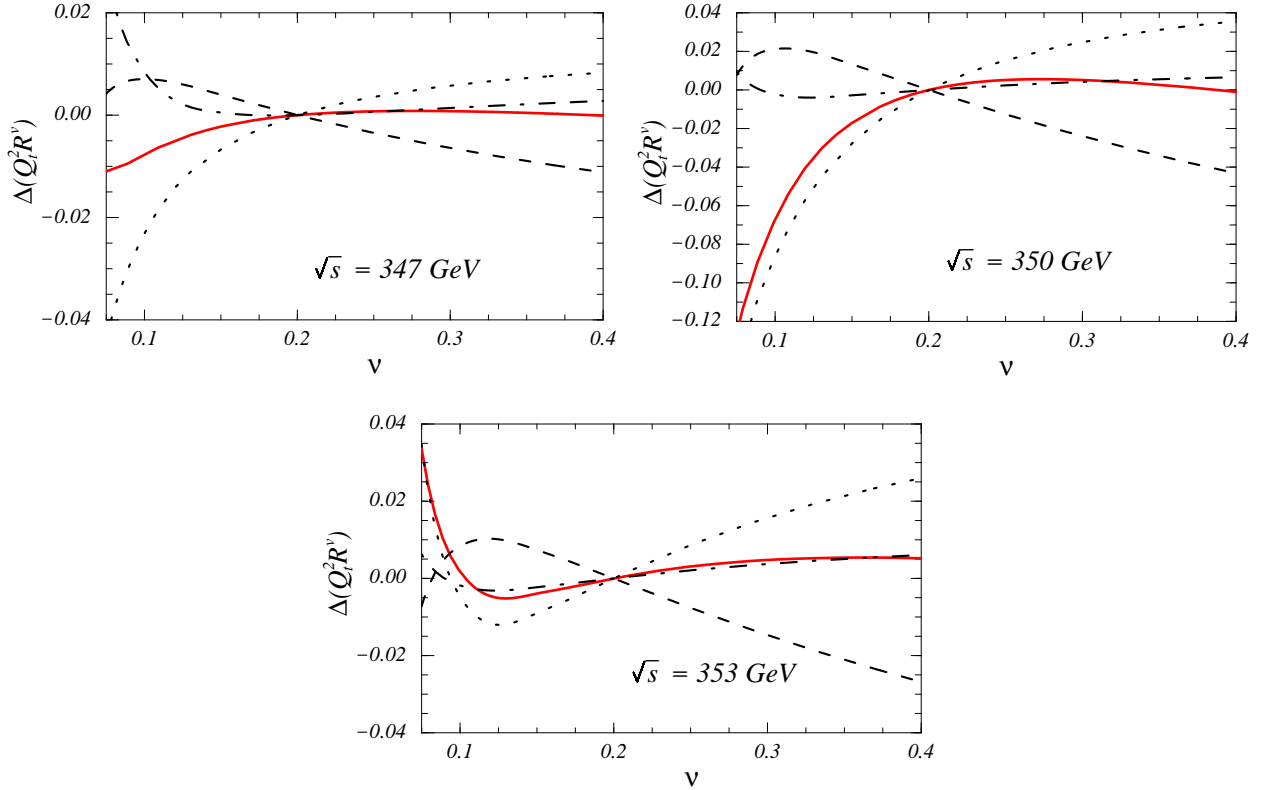


FIG. 7. Relative scale dependence of various NNLL contributions to $Q_t^2 R^\nu$. The contributions in Eq. (40) were divided into those from $G_{v,m,\nu}^c$ (dashed lines), δG^k (dotted lines), and the sum of $\delta G^{\delta,r,\text{kin},1\text{S}}$ (dot-dashed lines), while the solid lines denote the sum of these terms.

ν is still much larger than the variation of R^a . Therefore, to estimate the remaining overall uncertainty in $\sigma_{\text{tot}}^{\gamma,Z}$ the variation of R^a can be neglected, and for the rest of this section we discuss only R^ν .

First we wish to explore the origin of the reduced ν dependence. In Fig. 7a,b,c $Q_t^2 R^\nu$ (solid red line) is displayed as a function of ν for $\sqrt{s} = 347, 350, 353$ GeV, using the choice of parameters of Fig. 5. We have also displayed separately, the contributions to $Q_t^2 R^\nu$ coming from G^c (dashed line), δG^k (dotted line) and the sum of $\delta G^{\delta,r,\text{kin},1\text{S}}$ (dot-dashed line). For all curves in Fig. 7 the respective values at $\nu = 0.2$ have been subtracted. The results show that for any c.m. energy the ν -variation of the individual contributions to R^ν is much stronger than the ν -variation of the sum. As an example, for $\sqrt{s} = 350$ and $\nu > 0.15$, one finds that the variation of the contributions from G^c and δG^k cancels almost entirely, whereas the contribution from the sum $\delta G^{\delta,r,\text{kin},1\text{S}}$ is nearly ν -independent. On the other hand, for $\sqrt{s} = 350$ and $\nu < 0.2$ the ν -variation is dominated by the contribution from δG^k which rapidly decreases, whereas the contributions from G^c and $\delta G^{\delta,r,\text{kin},1\text{S}}$ are small. The situation is quite similar for other energies, and results directly from the evolution equation of the Wilson coefficients. These evolution equations constitute a system of coupled differential equations, where the values of the Wilson coefficients become related to each other for $\nu < 1$. This is different from the fixed order NNLO calculations carried out in previous

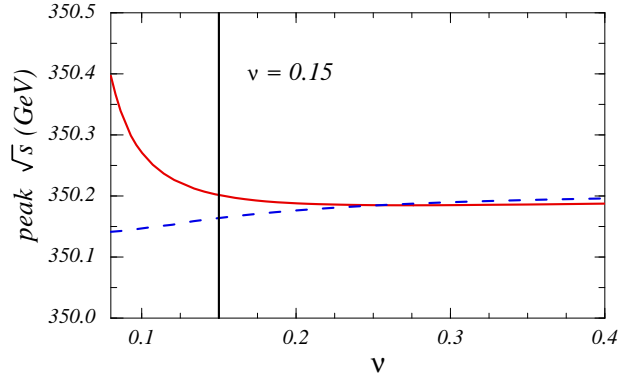


FIG. 8. Position of the peak in the cross-section versus ν at NNLO (dashed) and NNLL (solid). The vertical line at $\nu = 0.15$ is a physically motivated endpoint for the running.

works [10–16], where the proper anomalous dimensions of the potentials and currents were not taken into account, and where the Wilson coefficients at the soft scale were obtained from simply evaluating their hard matching conditions at the soft scale. In particular, in the fixed order approach, there is no numerical cancellation between the scale-dependence that arises from the corrections to the Coulomb potential \tilde{V}_c and the corrections from the potential \tilde{V}_k (see Eqs. (11) and (12)). In addition, in the fixed order approach, the contribution from \tilde{V}_k becomes quite large at low scales because it is proportional to the square of the strong coupling. In fact, in previous fixed order NNLO calculations \tilde{V}_k was identified as one of the major sources of the large positive corrections to the normalization of the total cross section. Using the VRG, on the other hand, the Wilson coefficient for \tilde{V}_k decreases by almost an order of magnitude between $\nu = 1$ and $\nu \sim 0.2$, and even vanishes for $\nu \approx 0.17$ [25]. This is one of the main reasons for the small size of the NNLL corrections. From the previous considerations we conclude that the cancellation of the ν -dependence and the size of the corrections that arises in the sum the various contributions to R^ν is a genuine and systematic QCD effect, and, in particular, that it is justified to take the overall ν -variation of R^ν as a tool to estimate the remaining theoretical uncertainties.

Let us now consider the range of ν that should be considered for a suitable error estimate. As mentioned before, from the physical point of view the appropriate choice of the subtraction velocity parameter ν is around $\alpha_s \approx 0.15$ – 0.2 . With this choice all large logarithms of ratios of the the hard scale m_t and the non-relativistic scales $m_t\nu$ and $m_t\nu^2$ are summed into the Wilson coefficients, whereas the matrix elements of vNRQCD operators are free of such logarithmic terms. From Fig. 6b we see that if the lower limit for ν is taken to be the endpoint of the running, $\nu \simeq 0.15$, then there is really only a very small uncertainty from the residual scale dependence. To be conservative we feel that the $\nu = 0.1$ curve should be included. The curves in Fig. 7 show that our results become unstable for $\nu \lesssim 0.1$. This is a consequence of the dependence of the VRG equations on the ultrasoft scale $\mu_U = m_t\nu^2$, which becomes of the order 1 GeV for $\nu \lesssim 0.1$. Thus, for $\nu \lesssim 0.1$ the perturbation expansion is apparently unreliable. However, this is just an artifact of choosing $m_t\nu^2$ much smaller than the physical energy scales in $\bar{t}t$, so that $\alpha_s(m_t\nu^2)$ is large. The same feature can also be observed in Fig. 8, where the position of the 1S peak is displayed as a function of ν for the parameter choice used previously. For $\nu \geq 0.15$ the peak position is stable, while for

$\nu \lesssim 0.1$ the peak position increases rapidly to higher energies. This is in contrast to the expectations in the 1S mass scheme, where the peak position should be stable by construction. The behavior of the peak position for $\nu \lesssim 0.1$ is a consequence of our perturbative treatment of the corrections that arise from the $1/m$ -suppressed potentials and the kinetic energy correction. For $\nu \lesssim 0.1$ these corrections become large and render the perturbative treatment unreliable. Thus, we conclude that the range $\nu \lesssim 0.1$ should not be used for the estimate of the remaining theoretical uncertainties.

As far as values of ν larger than 0.2 are concerned the curves in Figs. 5–8 show that our results are remarkably stable up to quite large values of the subtraction velocity, even beyond $\nu = 0.4$. For the estimate of the remaining theoretical uncertainty of the total cross section it is therefore not mandatory to fix any strict upper bound of ν . In Table. I we have shown results for $\nu = 0.1, 0.125, 0.2, 0.275,$ and 0.4 . We consider the small value, $\nu = 0.1$, as a conservative lower bound, which is set by physical considerations, and below which no sensible perturbative treatment is possible. A less conservative approach would have been to take the lower bound to be set by the typical top quark velocity, $\nu \simeq 0.15 - 0.2$. The value $\nu = 0.275$, on the other hand, has been included because for this choice the peak cross section reaches its maximum as a function of ν . We take the size of the resulting ν -variation of the cross section at the 1S peak,

$$\frac{\delta\sigma_{t\bar{t}}}{\sigma_{t\bar{t}}} = \pm 3\% \quad (51)$$

as the remaining uncertainty inherent to our renormalization group improved calculation. This is an order of magnitude smaller than the uncertainty that was associated to previous fixed order NNLO QCD calculations of the cross section. Note that if $\nu = 0.125$ was instead used as the lower bound for the running then the ν -variation is $\delta\sigma_{t\bar{t}}/\sigma_{t\bar{t}} = \pm 1.5\%$. In fact, the small ν -dependence and the small size of the NNLL order corrections observed in our calculation of the cross section comply with the expectations from power counting and the natural notion that the non-relativistic $t\bar{t}$ dynamics should be calculable to a high degree of precision [1, 2].

It is instructive to compare the error assigned to the cross section based on the ν -variation with the size of corrections from terms that are not yet included in our NNLL result. Firstly, at NNLL the complete running of $c_1(\nu)$ was not included because the three loop anomalous dimension for $c_1(\nu)$ is not yet completely known. (We recall that already at NLL order $[c_1(\nu \approx \alpha_s)]^2$ contains the sizeable negative (fixed order) N³LO normalization correction proportional to $\alpha_s^3 \ln^2 \alpha_s$ that was determined in Ref. [20], see Ref. [25].) Contributions to the three loop anomalous dimension are discussed in Appendix A 2, and based on dimensional analysis and the known contributions to this anomalous dimension we estimate that the uncertainty in neglecting it is $\lesssim 2\%$. It is also useful to consider the size of some corrections from beyond NNLL that can be determined easily or have been obtained earlier. We emphasize that all such corrections belong to matrix elements of the effective theory, i.e. it is crucial to employ the proper choice for the renormalization scale μ_S or μ_U depending on whether the corrections come from the soft (or potential) or ultrasoft momentum regime. Let us first consider the corrections arising from two insertions of \tilde{V}_δ (at second order time-independent perturbation theory). As the correction arises from potential momenta the soft renormalization scale has to be used. We find that the relative corrections are at most 2.8%

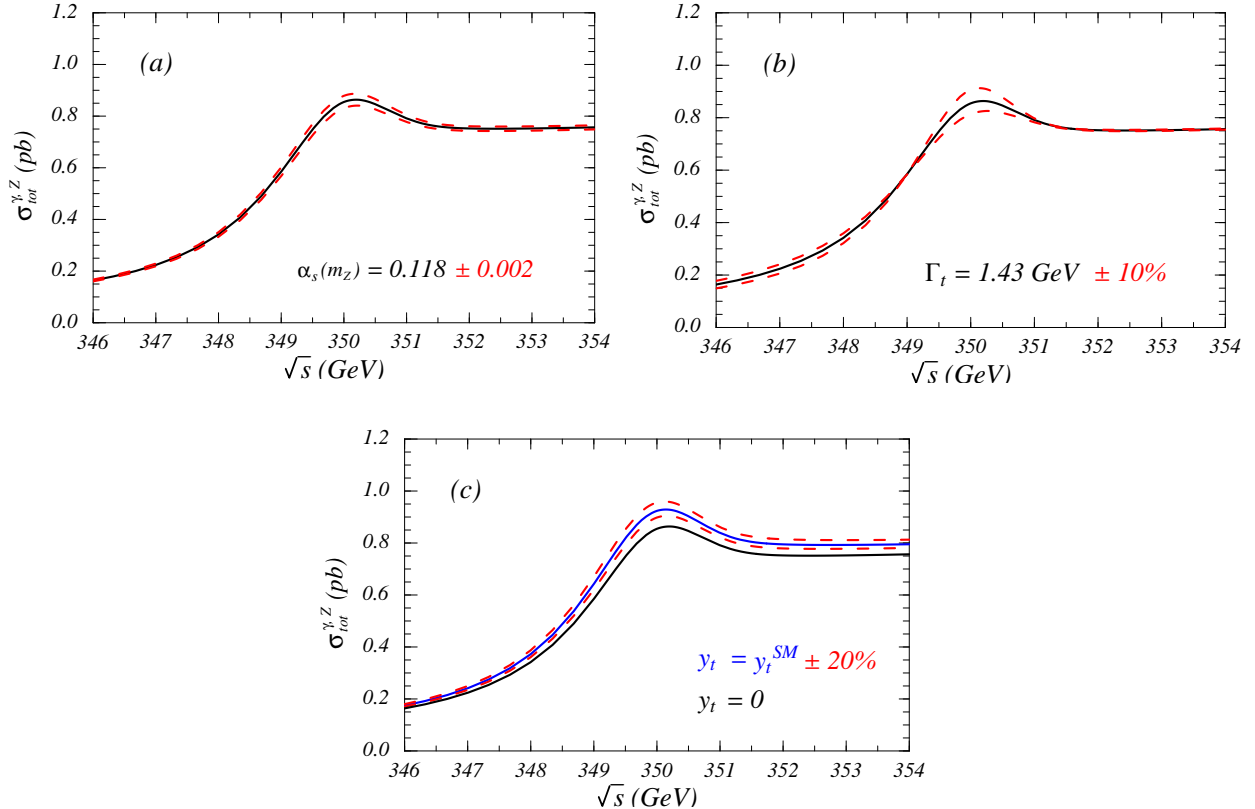


FIG. 9. Variation of the NNLL cross section for a) the value of the strong coupling, b) the top quark width, and c) the inclusion of a Standard Model (SM) Higgs boson. Changes relative to the central value (solid lines) are shown by dashed red lines. In c) there are two solid lines, the lower black line is the decoupling limit for the Higgs boson, and the upper blue line is for a SM Higgs with mass $m_H = 115$ GeV.

(for $\nu = 0.1$ and close to the peak). In Ref. [58] the corrections to the square of the S -wave quarkonium wavefunction at the origin arising from the emission and reabsorption of an ultrasoft gluon were determined. Naturally the ultrasoft scale has to be used in this case. These corrections can be taken as an estimate for the ultrasoft corrections to the normalization of the total cross section. For the ground state ($n = 1$) one finds that this ultrasoft correction amounts to about 2% for $\nu \approx \alpha_s$. This is also consistent with our error estimate.

VIII. PHENOMENOLOGICAL CONSEQUENCES

Our result for the total cross section confirms the previous result in the fixed order approach that a top quark mass measurement with theoretical uncertainties at the level of 100 – 200 MeV or better is feasible [17]. In principle, the prospects are now even better, because the small normalization uncertainties of the renormalization group improved calculation have eliminated the danger that normalization uncertainties could feed into the top mass measurement through beam effects caused by initial state radiation, beam en-

ergy smearing, and beam-strahlung. On the other hand, it is also natural to reconsider the threshold scan as an instrument to carry out precise measurements of other top quark parameters such as the strong coupling α_s , the top Yukawa coupling y_t or the total top width Γ_t – ideas that have not been seriously considered since the large NNLO corrections to the normalization of the cross section were discovered. In fact, in view of our renormalization group improved NNLL calculation, older studies assessing how precise these parameters can be measured (see e.g. Refs. [8,9]), appear more realistic than conclusions based on the NNLO predictions.

Here we discuss the sensitivity of the total cross section $\sigma_{\text{tot}}^{\gamma,Z}$ to changes in the input parameters $\alpha_s^{n_l=5}(m_Z)$, Γ_t , and y_t (for a light Higgs). Our discussion is restricted to the Standard Model. However, we note that low energy supersymmetry does not lead to considerable changes in the QCD dynamics [59], even though it can lead to modifications of the value of electroweak parameters that can be measured at the top threshold such as Γ_t and y_t . For the implementation of the Higgs effects we use the prescription of Ref. [60]. For Higgs mass m_H , the Higgs potential

$$\tilde{V}_{tth}(\mathbf{p}, \mathbf{q}) = -\frac{y_t^2}{2} \frac{1}{\mathbf{k}^2 + m_H^2} \quad (52)$$

is accounted for exactly through Eq. (35), and the one-loop short-distance corrections to the current $\mathbf{O}_{p,1}$ that depend on y_t are included in the matching condition $c_1(1)$ [60]

$$c_1(1) \rightarrow c_1(1) \left[1 + \frac{y_t^2}{8\pi^2} \left(1 - \frac{r}{3} - \frac{\pi}{\sqrt{r}} + \left(1 - \frac{3r}{4} + \frac{r^2}{6} \right) \ln r \right. \right. \\ \left. \left. + \sqrt{(4-r)r} \left(\frac{1}{r} - \frac{5}{6} + \frac{r^2}{3} \right) \cos^{-1} \left(\frac{\sqrt{r}}{2} \right) \right], \quad (53)$$

where $r = m_H/m_t$. Assuming that m_H has been measured elsewhere, the question to address from the top threshold cross-section is how well y_t can be measured.

In Figs. 9 we have displayed the variation of the NNLL cross section $\sigma_{\text{tot}}^{\gamma,Z}$ as a function of \sqrt{s} for different choices of the input parameters $\alpha_s(m_Z)$, Γ_t and y_t . In all figures we have chosen $M_t^{\text{1S}} = 175$ GeV, $\Gamma_t = 1.43$ GeV, $\alpha_s(m_Z) = 0.118$, $y_t = 0$ and $\nu = 0.15$, unless stated otherwise. The upper left panel shows the cross section for 0.116 (lower dashed red line), 0.118 (solid black line), and 0.120 (upper dashed red line). At the peak one finds a $\pm 2.7\%$ variation when varying $\alpha_s(m_Z)$ by ± 0.002 . The upper right panel shows the cross section for $\Gamma_t = 1.43$ GeV (solid black line). The dashed red lines correspond to variations of Γ_t by $\pm 10\%$, where for a smaller width the peak becomes more pronounced. At the peak one finds a $(-2.3\%, +2.6\%)$ variation of the cross section when varying Γ_t by $\pm 5\%$. Finally, the lower panel shows the cross section for zero Yukawa coupling (solid black line), the Standard Model value for the Yukawa coupling (solid blue line), and a $\pm 20\%$ variation of the coupling with respect to the SM value (upper/lower dashed red lines). The Higgs mass was chosen to be $m_H = 115$ GeV. At the peak one finds a $(+3.3\%, -2.6\%)$ variation when varying y_t^{SM} by $\pm 20\%$. For $m_H = 130$ and 150 GeV the corresponding variations are $(+2.9\%, -2.3\%)$ and $(+2.5\%, -2.0\%)$ respectively.

Thus, given the remaining 3% uncertainty from higher order QCD effects, measurements with uncertainties of $\delta\alpha_s(m_Z) \sim 0.002$, $\delta\Gamma_t/\Gamma_t \sim 5\%$ and $\delta y_t/y_t \sim 20\%$ appear feasible. More

accurate extractions might be possible if better use is made of the smaller scale dependence above and below the 1S peak. A detailed simulation study based on the NNLL results will be necessary to more realistically assess the uncertainties in measurements of α_s , Γ_t and y_t . Such a simulation is beyond the scope of this work.

Finally, we comment on other prospects for measurements of α_s , Γ_t , and y_t . Extractions of α_s from many processes currently have a combined ± 0.002 – 0.003 uncertainty [61,62], but in the very long term a 1% uncertainty may be achievable [63,64]. Measurements of the forward-backward asymmetry and momentum distribution for top quarks near threshold may help to reduce the uncertainty in an extraction of Γ_t [8,9]. The top Yukawa coupling can also be measured above threshold from $e^+e^- \rightarrow t\bar{t}h$ [65]. However, at $\sqrt{s} = 500$ GeV the phase space for this process is restricted, so precise extractions above threshold require a 0.8–1 TeV linear collider and high luminosity.

IX. SUMMARY AND OUTLOOK

In this work we have studied the impact of the summation of QCD logarithms of ratios of the scales m_t , m_tv and m_tv^2 on the total top pair production cross section in the kinematic regime close to threshold. Using the recently developed effective field theory vNRQCD [22–25] the logarithms of velocity are summed in the Wilson coefficients of the vNRQCD operators based on renormalization group equations that are determined from the anomalous dimensions of the nonrelativistic operators. All NNLL terms were accounted for, except for the Wilson coefficient c_1 of the dimension three production current for which only NLL results are completely available [25]. Based on partial contributions to the three loop anomalous dimension that are currently known, the modification of c_1 at NNLL order was estimated to be at the 1% level. We find that the size of the NNLL corrections and the variation of the NNLL cross section for different choices of the scaling parameter ν is an order of magnitude smaller than the results of earlier NNLO calculations [17], where the logarithmic terms were not summed. We conclude that a conservative estimate of the remaining theoretical QCD uncertainty of the normalization of the cross section is $\pm 3\%$. The already excellent prospects of a top quark mass measurement at the level of 100–200 MeV or better [17], are in principle further improved because the danger that normalization uncertainties could feed into the top mass measurement through beam smearing effects is eliminated. Also, measurements of α_s , Γ_t and y_t from a threshold scan with theoretical uncertainties of about $\delta\alpha_s(m_Z) \sim 0.002$, $\delta\Gamma_t/\Gamma_t \sim 5\%$ and $\delta y_t/y_t \sim 20\%$ appear feasible at this stage. However, realistic simulation studies are still necessary to obtain more definite numbers.

At the level of uncertainty of our computation of the total cross section there are additional subleading effects which should be reconsidered. Many small effects were previously considered irrelevant for the total cross section due to the large size of the QCD corrections found at NNLO. Here, let us just mention electroweak effects. The dominant contribution was included and comes from the top width, which is the reason that the threshold top cross section is a smooth lineshape and can be calculated for all center of mass energies. At subleading order a number of additional effects need to be taken into account, such as the so-called non-factorizable corrections [30], electroweak box and triangle diagrams [66], W -width effects [67], and single- or non-resonant background processes that lead to the same final state as top pair production and phase space corrections [15]. These corrections lead

to effects at the percent level and are expected to be of the same size as the remaining QCD uncertainties.

X. ACKNOWLEDGEMENT

AM and IS are supported in part by the U.S. Department of Energy under contract DOE DE-FG03-97ER40546. TT is supported in part by BMBF contract no. 05-HT1-PAA-4. IS would like to thank A. Falk for useful discussion.

APPENDIX A: CONSTANTS AND RUNNING COUPLINGS

1. Formulæ for constants

In this appendix expressions for the constants that appear in the effective Coulomb potential $\tilde{V}_c(\mathbf{p}, \mathbf{q})$ are collected and the two loop matching for $c_1(1)$ is discussed. The β -functions and constant coefficients which appear in $\tilde{V}_c(\mathbf{p}, \mathbf{q})$ in Eq. (11) include

$$\begin{aligned}
\beta_0 &= \frac{11}{3} C_A - \frac{4}{3} T_F n_l, \\
\beta_1 &= \frac{34}{3} C_A^2 - \frac{20}{3} C_A T_F n_l - 4 C_F T_F n_l, \\
a_1 &= \frac{31}{9} C_A - \frac{20}{9} T_F n_l, \\
a_2 &= \left(\frac{4343}{162} + 4\pi^2 - \frac{\pi^4}{4} + \frac{22}{3} \zeta_3 \right) C_A^2 - \left(\frac{1798}{81} + \frac{56}{3} \zeta_3 \right) C_A T_F n_l \\
&\quad - \left(\frac{55}{3} - 16 \zeta_3 \right) C_F T_F n_l + \left(\frac{20}{9} T_F n_l \right)^2,
\end{aligned} \tag{A1}$$

where the a_2 term was computed in Ref. [36], and $n_l = 5$ is the number of light fermions.

For the matching onto the coefficient $c_1(1)$ of the non-relativistic current $\mathbf{O}_{\mathbf{p},1}$ in Eq. (14), the one-loop contribution is well known. The two-loop computation involves computing the difference of graphs in full QCD and the effective theory as shown in Fig. 10. We find

$$\begin{aligned}
c_1(1) &= 1 - \frac{2C_F}{\pi} \alpha_s(m) + \alpha_s^2(m) \left[C_F^2 \left(\frac{\ln 2}{12} - \frac{25}{24} - \frac{2}{\pi^2} \right) + C_A C_F (\ln 2 - 1) + \frac{\kappa}{2} \right], \\
\kappa &= C_F^2 \left[\frac{1}{\pi^2} \left(\frac{39}{4} - \zeta_3 \right) + \frac{4}{3} \ln 2 - \frac{35}{18} \right] - C_A C_F \left[\frac{1}{\pi^2} \left(\frac{151}{36} + \frac{13}{2} \zeta_3 \right) + \frac{8}{3} \ln 2 - \frac{179}{72} \right] \\
&\quad + C_F T_F \left[\frac{4}{9} \left(\frac{11}{\pi^2} - 1 \right) \right] + C_F T_F n_l \left[\frac{11}{9\pi^2} \right].
\end{aligned} \tag{A2}$$

At order $\alpha_s(m)^2$ this matching result is scheme dependent and depends both on the subtraction scheme as well as on the definition of operators in the effective theory. For this reason the result in Eq. (A2) differs from the earliest results in Refs. [28, 29] for $c_1(1)$. In

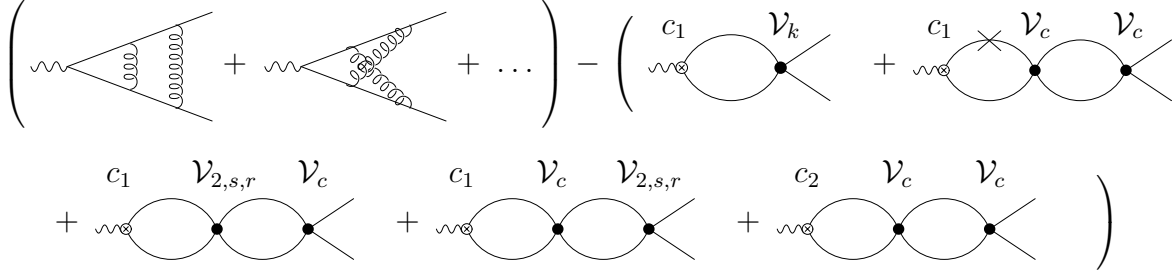


FIG. 10. Difference of full QCD [11] and order $\alpha_s^2 v^0$ EFT graphs which gives the two loop matching for $c_1(1)$. The \times denotes an insertion of the $\mathbf{p}^4/(8m^3)$ operator, and graphs with this insertion on a different propagator are understood.

Refs. [28,29] the potential operators in Eq. (12) were defined with dependence on $d = 4 - 2\epsilon$ in such a way that only the hard part of the two loop graphs in the threshold expansion contributed. The result in Eq. (A2) uses the $\overline{\text{MS}}$ scheme with all effective theory operators defined on-shell in $d = 4$ space-time dimensions. The full theory result was extracted from Ref. [28], while the EFT graphs were computed explicitly. We have obtained the same result by using the “direct matching” of Ref. [68], where one matches results for cross sections in the full and effective theories rather than matching the Green functions.

2. Formulæ for running couplings

In this section the formulæ for the Wilson coefficients of operators needed for our NNLL cross section are given. The Wilson coefficients for the potential operators in Eqs. (11) and (12) were computed in Refs. [23, 25, 26], and due to mixing depend on the one-loop running of the HQET $1/m^2$ terms computed in Ref. [69]. For completeness we summarize the results for the color singlet coefficients:

$$\begin{aligned} \mathcal{V}_c^{(s)}(\nu) &= -4\pi C_F z \alpha_s(m) + \frac{8\pi C_F C_A^3}{3\beta_0} \left[\frac{11}{4} - 2z - \frac{z^2}{2} - \frac{z^3}{4} + 4 \ln(w) \right] \alpha_s^3(m), \\ \mathcal{V}_k^{(s)}(\nu) &= C_F \left(\frac{C_F}{2} - C_A \right) z^2 \alpha^2(m) + \frac{8C_F C_A (C_A + 2C_F)}{3\beta_0} \left[4 - 3z - z^2 + 6 \ln(w) \right] \alpha_s^2(m), \\ \mathcal{V}_2^{(s)}(\nu) &= C_F \pi \left\{ \frac{235C_A^2 - 716C_F C_A + 99\beta_0 C_A + 96\beta_0 C_F}{39\beta_0 C_A} [z - 1] \right. \\ &\quad - \frac{(\beta_0 - 5C_A)}{(\beta_0 - 2C_A)} \left[z^{(1-2C_A/\beta_0)} - 1 \right] - \frac{8(3\beta_0 - 11C_A)(5C_A + 8C_F)}{13(6\beta_0 - 13C_A)C_A} \left[z^{(1-13C_A/(6\beta_0))} - 1 \right] \\ &\quad \left. - \frac{32(C_A - 2C_F)}{3\beta_0} \ln(w) \right\} \alpha_s(m), \\ \mathcal{V}_s^{(s)}(\nu) &= \frac{-2\pi C_F}{(2C_A - \beta_0)} \left[C_A + \frac{1}{3} (2\beta_0 - 7C_A) z^{(1-2C_A/\beta_0)} \right] \alpha_s(m), \end{aligned}$$

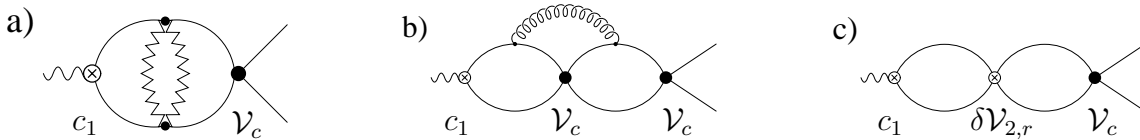


FIG. 11. Examples of the type of graphs that contribute to the three-loop anomalous dimension for c_1 . $\delta\mathcal{V}_{2,r}$ are one loop counterterms.

$$\mathcal{V}_r^{(s)}(\nu) = -4\pi C_F z \alpha_s(m) + \frac{32\pi C_F C_A}{3\beta_0} [1 - z] \alpha_s(m) + \frac{64\pi C_F C_A}{3\beta_0} \ln(w) \alpha_s(m), \quad (\text{A3})$$

where

$$z = \frac{\alpha_s(m\nu)}{\alpha_s(m)}, \quad w = \frac{\alpha_s(m\nu^2)}{\alpha_s(m\nu)}. \quad (\text{A4})$$

Next consider the Wilson coefficients of the currents in Eqs. (14) and (15). The LL solutions are $c_1(\nu) = c_3(\nu) = 1$, while the solution for $c_2(\nu)$ is given in Eq. (19). The NLL solution for $c_1(\nu)$ is obtained by integrating the two-loop anomalous dimension [22]

$$\nu \frac{\partial}{\partial \nu} \ln[c_1(\nu)] = -\frac{\mathcal{V}_c^{(s)}(\nu)}{16\pi^2} \left(\frac{\mathcal{V}_c^{(s)}(\nu)}{4} + \mathcal{V}_2^{(s)}(\nu) + \mathcal{V}_r^{(s)}(\nu) + 2\mathcal{V}_s^{(s)}(\nu) \right) + \frac{\mathcal{V}_k^{(s)}(\nu)}{2}, \quad (\text{A5})$$

with one-loop matching. The analytic solution of Eq. (A5) can be found in Ref. [25].

At NNLL we use the two-loop matching in Eq. (A2), however the complete three-loop anomalous dimension is currently unknown. Part of the unknown contributions are due to the mixing in Eq. (A5). Solving for the full NNLL $c_1(\nu)$ requires the NLL values of $\mathcal{V}_c(\nu)$, $\mathcal{V}_2(\nu)$, $\mathcal{V}_r(\nu)$ and $\mathcal{V}_s(\nu)$, and the NNLL value of $\mathcal{V}_k(\nu)$, which in turn require knowing the running of $1/m^2$ operators in the HQET Lagrangian at two-loops. Note that at one-loop, the calculation of the full mixing matrix in Ref. [69] already involved 75 diagrams. In addition there are direct contributions to the three loop anomalous dimension from three-loop graphs with divergences which require a c_1 counterterm. By power counting we find that there are no contributions from purely potential three loop diagrams. However, diagrams with soft and ultrasoft gluons such as those shown in Fig. 11 may contribute. Graphs with ultrasoft gluons are expected to generate an anomalous dimension of the form

$$\gamma_{\text{us}} = \lambda \frac{\alpha_s(m\nu^2) [\mathcal{V}_c^{(s)}(\nu)]^2}{64\pi^3} \quad (\text{A6})$$

where λ is (currently) an unknown number. A complete calculation of λ may not be that difficult, and is of interest since the graphs with soft gluons give contributions which are parametrically smaller by a factor $\alpha_s(m\nu)/\alpha_s(m\nu^2)$.

Interestingly, we note that the cancellation of subdivergences $\ln(p)/\epsilon$ and $\ln(E)/\epsilon$ between Fig. 11b and the counterterm graph in Fig. 11c *requires* the velocity renormalization group relation $\mu_U = \mu_S^2/m$ for consistency. In Coulomb gauge

$$\begin{aligned}
\text{Fig. 11b} &= \frac{\alpha_s(m\nu^2)[\mathcal{V}_c(\nu)]^2}{192\pi^3} \left(C_F - \frac{C_A}{2} \right) \left[\frac{1}{4\epsilon^2} + \frac{1}{4\epsilon} \ln\left(\frac{\mu_U^2}{E^2}\right) + \frac{1}{2\epsilon} \ln\left(\frac{\mu_S^2}{p^2}\right) + \frac{\#}{\epsilon} + \text{finite} \right], \\
\text{Fig. 11c} &= -\frac{\alpha_s(m\nu^2)[\mathcal{V}_c(\nu)]^2}{192\pi^3} \left(C_F - \frac{C_A}{2} \right) \left[\frac{1}{2\epsilon^2} + \frac{1}{\epsilon} \ln\left(\frac{\mu_S^2}{p^2}\right) + \frac{\#}{\epsilon} + \text{finite} \right]. \tag{A7}
\end{aligned}$$

It is easy to see that the subdivergences of the form $\ln(\dots)/\epsilon$ cancel completely *only* after using the equations of motion $E = p^2/m$ and $\mu_U = \mu_S^2/m$. The difference of $\#/\epsilon$ terms in Eq. (A7) will contribute to Eq. (A6). If only a single μ were used then one would be left with a $\ln(\mu/m)$ term contributing to the anomalous dimension which is obviously wrong.

To numerically estimate the effect of the three loop anomalous dimension on $c_1(\nu)$ we consider several types of contributions:

1. At NLL the running of $\mathcal{V}_c^{(s)}(\nu)$ is determined by the two-loop β -function, so a subset of terms in the anomalous dimension are determined by increasing the order of the running used for α_s . Using one-loop running for z and w in Eq. (A4) gives $c_1^{\text{NNLL}}(\nu = 0.15) = 0.8970$, whereas two-loop running gives $c_1^{\text{NNLL}}(\nu = 0.15) = 0.8941$.
2. Another estimate comes from partial knowledge of the NLL results for $\mathcal{V}_{2,s}^{(s)}(\nu)$ and the NNLL result for $\mathcal{V}_k^{(s)}(\nu)$ which enter in Eq. (A5). The matching for these potentials is known, however the complete anomalous dimensions are not. The one-loop matching values are [24, 70] $\mathcal{V}_2^{(s)}(1) = 241/135 \alpha_s^2(m)$ and $\mathcal{V}_s^{(s)}(1) = 112/27 \alpha_s^2(m)$. The recently computed two-loop matching [71] for the $1/|\mathbf{k}|$ potential gives $\mathcal{V}_k(1) = -(289 + 4896 \ln 2)/(324\pi) \alpha_s^3(m)$. Furthermore, the QED anomalous dimensions for these potentials are known [33], and directly give a majority of the purely potential contributions to the QCD anomalous dimensions (in the notation of Ref. [33] we include the terms $\rho_{ccc}, \rho_{cc2}, \rho_{c22}, \rho_{ck},$ and ρ_{k2}). Using these results as approximations for $\mathcal{V}_{2,s}^{(s)\text{NLL}}(\nu)$ and $\mathcal{V}_k^{(s)\text{NNLL}}(\nu)$, and then including these contributions in Eq. (A5) gives $c_1^{\text{NNLL}}(\nu = 0.15) = 0.8991$. The result without the two-loop matching from Ref. [71] is $c_1^{\text{NNLL}}(\nu = 0.15) = 0.8915$.
3. Finally, adding a contribution of the form in Eq. (A6) with $\lambda = \pm 5$ to account for the possibility of a large coefficient gives the range $c_1^{\text{NNLL}}(\nu = 0.15) = 0.8903$ to 0.8969 (using three loop running for α_s).

Adding the magnitude of these three anomalous dimension contributions linearly, we find a 1.2% change in $c_1(\nu = 0.15)$ relative to the NNLL value which includes only the two-loop matching for c_1 . We therefore do not expect that the missing three loop anomalous dimension for c_1 will shift the value of R^v by more than an amount at the 2% level.

REFERENCES

- [1] J. H. Kühn, in *C80-05-29.6 Acta Phys. Polon.* **B12**, 347 (1981); I. I. Bigi, Y. L. Dokshitzer, V. Khoze, J. Kühn and P. Zerwas, *Phys. Lett.* **B181**, 157 (1986).
- [2] V. S. Fadin and V. A. Khoze, *JETP Lett.* **46**, 525 (1987).
- [3] M. J. Strassler and M. E. Peskin, *Phys. Rev.* **D43**, 1500 (1991).
- [4] M. Jeżabek, J. H. Kühn and T. Teubner, *Z. Phys.* **C56**, 653 (1992).
- [5] Y. Sumino, K. Fujii, K. Hagiwara, H. Murayama and C. K. Ng, *Phys. Rev.* **D47**, 56 (1993).
- [6] H. Murayama and Y. Sumino, *Phys. Rev.* **D47**, 82 (1993); R. Harlander, M. Jeżabek, J. H. Kühn and T. Teubner, *Phys. Lett.* **B346**, 137 (1995) [hep-ph/9411395];
- [7] R. Harlander, M. Jeżabek, J. H. Kühn and M. Peter, *Z. Phys.* **C73**, 477 (1997) [hep-ph/9604328]; M. Peter and Y. Sumino, *Phys. Rev.* **D57**, 6912 (1998) [hep-ph/9708223].
- [8] K. Fujii, T. Matsui and Y. Sumino, *Phys. Rev.* **D50**, 4341 (1994).
- [9] P. Comas, R. Miquel, M. Martinez and S. Orteu, talk published in *e^+e^- Linear Collisions at 500 GeV*, DESY 96-123D (1996) 57.
- [10] A. H. Hoang and T. Teubner, *Phys. Rev.* **D58**, 114023 (1998) [hep-ph/9801397].
- [11] K. Melnikov and A. Yelkhovsky, *Nucl. Phys.* **B528**, 59 (1998) [hep-ph/9802379].
- [12] O. Yakovlev, *Phys. Lett.* **B457**, 170 (1999) [hep-ph/9808463].
- [13] M. Beneke, A. Signer and V. A. Smirnov, *Phys. Lett.* **B454**, 137 (1999) [hep-ph/9903260].
- [14] T. Nagano, A. Ota and Y. Sumino, *Phys. Rev.* **D60**, 114014 (1999) [hep-ph/9903498].
- [15] A. H. Hoang and T. Teubner, *Phys. Rev.* **D60**, 114027 (1999) [hep-ph/9904468].
- [16] A. A. Penin and A. A. Pivovarov, *Nucl. Phys.* **B550**, 375 (1999) [hep-ph/9810496]; *Phys. Atom. Nucl.* **64**, 275 (2001) [*Yad. Fiz.* **64**, 323 (2001)] [hep-ph/9904278].
- [17] A. H. Hoang *et al.*, in *Eur. Phys. J. direct* **C3**, 1 (2000) [hep-ph/0001286].
- [18] D. Peralta, M. Martinez and R. Miquel, talk presented at the *4th International Workshop on Linear Colliders*, Sitges, Barcelona, Spain, April 28 - May 5 1999.
- [19] G. Buchalla, A. J. Buras and M. E. Lautenbacher, *Rev. Mod. Phys.* **68**, 1125 (1996) [hep-ph/9512380].
- [20] B. A. Kniehl and A. A. Penin, *Nucl. Phys.* **B577**, 197 (2000) [hep-ph/9911414].
- [21] A. H. Hoang, A. V. Manohar, I. W. Stewart and T. Teubner, *Phys. Rev. Lett.* **86**, 1951 (2001) [hep-ph/0011254].
- [22] M. E. Luke, A. V. Manohar and I. Z. Rothstein, *Phys. Rev.* **D61**, 074025 (2000) [hep-ph/9910209].
- [23] A. V. Manohar and I. W. Stewart, *Phys. Rev.* **D62**, 014033 (2000) [hep-ph/9912226].
- [24] A. V. Manohar and I. W. Stewart, *Phys. Rev.* **D62**, 074015 (2000) [hep-ph/0003032].
- [25] A. V. Manohar and I. W. Stewart, *Phys. Rev.* **D63**, 054004 (2001) [hep-ph/0003107].
- [26] A. H. Hoang, A. V. Manohar and I. W. Stewart, *Phys. Rev.* **D64**, 014033 (2001) [hep-ph/0102257].
- [27] A. H. Hoang, *Phys. Rev.* **D56**, 7276 (1997) [hep-ph/9703404].
- [28] A. Czarnecki and K. Melnikov, *Phys. Rev. Lett.* **80**, 2531 (1998) [hep-ph/9712222].
- [29] M. Beneke, A. Signer and V. A. Smirnov, *Phys. Rev. Lett.* **80**, 2535 (1998) [hep-ph/9712302].
- [30] K. Melnikov and O. Yakovlev, *Phys. Lett.* **B324**, 217 (1994) [hep-ph/9302311];

- V. S. Fadin, V. A. Khoze and A. D. Martin, Phys. Rev. **D49**, 2247 (1994); W. Beenakker, F. A. Berends and A. P. Chapovsky, Phys. Lett. **B454**, 129 (1999) [hep-ph/9902304].
- [31] A. V. Manohar and M. B. Wise, *Cambridge Monographs on Particle Physics, Nuclear Physics, and Cosmology, Vol. 10*.
- [32] M. Beneke and V. A. Smirnov, Nucl. Phys. **B522**, 321 (1998) [hep-ph/9711391].
- [33] A. V. Manohar and I. W. Stewart, Phys. Rev. Lett. **85**, 2248 (2000) [hep-ph/0004018].
- [34] A. V. Manohar, J. Soto and I. W. Stewart, Phys. Lett. **B486**, 400 (2000) [hep-ph/0006096].
- [35] A. Pineda and J. Soto, Nucl. Phys. Proc. Suppl. **64**, 428 (1998);
- [36] M. Peter, Phys. Rev. Lett. **78**, 602 (1997) [hep-ph/9610209], corrected by Y. Schröder, Phys. Lett. **B447**, 321 (1999) [hep-ph/9812205].
- [37] M. J. Savage, K. A. Scaldeferri and M. B. Wise, Nucl. Phys. A **652**, 273 (1999) [nucl-th/9811029].
- [38] M. Luke and M. J. Savage, Phys. Rev. **D57**, 413 (1998) [hep-ph/9707313].
- [39] A. Denner and T. Sack, Nucl. Phys. **B358**, 46 (1991); W. Beenakker et al., Nucl. Phys. **B411**, 343 (1994); G. Eilam, R. R. Mendel, R. Migneron and A. Soni, Phys. Rev. Lett. **66**, 3105 (1991).
- [40] A. Czarnecki and K. Melnikov, Nucl. Phys. **B544**, 520 (1999) [hep-ph/9806244]; K. G. Chetyrkin et al., Phys. Rev. **D60**, 114015, (1999) [hep-ph/9910339].
- [41] M. B. Voloshin, Nucl. Phys. **B154**, 365 (1979).
- [42] H. Leutwyler, Phys. Lett. **B98**, 447 (1981).
- [43] M. Beneke, Nucl. Phys. Proc. Suppl. **86**, 547 (2000) [hep-ph/9910534].
- [44] V. S. Fadin and O. I. Yakovlev, Sov. J. Nucl. Phys. **53**, 688 (1991) [Yad. Fiz. **53**, 1111 (1991)].
- [45] E. H. Wichmann and C. H. Woo, J. Math. Phys. **2**, 178 (1961); L. Hostler, J. Math. Phys. **5**, 591 (1964); J. Schwinger, J. Math. Phys. **5**, 1606 (1964).
- [46] D. Eiras and J. Soto, Phys. Rev. **D61**, 114027 (2000) [hep-ph/9905543].
- [47] J. H. Kühn and T. Teubner, Eur. Phys. J. **C9**, 221 (1999) [hep-ph/9903322].
- [48] A. H. Hoang, Z. Ligeti and A. V. Manohar, Phys. Rev. Lett. **82**, 277 (1999) [hep-ph/9809423]; Phys. Rev. **D59**, 074017 (1999) [hep-ph/9811239].
- [49] A. S. Kronfeld, Phys. Rev. **D58**, 051501 (1998) [hep-ph/9805215].
- [50] R. Tarrach, Nucl. Phys. **B183**, 384 (1981).
- [51] M. Beneke and V. M. Braun, Nucl. Phys. **B426**, 301 (1994) [hep-ph/9402364]; I. I. Bigi, M. A. Shifman, N. G. Uraltsev and A. I. Vainshtein, Phys. Rev. **D50**, 2234 (1994) [hep-ph/9402360].
- [52] U. Aglietti and Z. Ligeti, Phys. Lett. **B364**, 75 (1995) [hep-ph/9503209].
- [53] A. H. Hoang, M. C. Smith, T. Stelzer and S. Willenbrock, Phys. Rev. **D59**, 114014 (1999) [hep-ph/9804227].
- [54] M. Beneke, Phys. Lett. **B434**, 115 (1998) [hep-ph/9804241].
- [55] I. Bigi, M. Shifman, N. Uraltsev and A. Vainshtein, Phys. Rev. **D56**, 4017 (1997) [hep-ph/9704245].
- [56] O. Yakovlev and S. Groote, hep-ph/0008156.
- [57] A. H. Hoang, hep-ph/0008102.
- [58] B. A. Kniehl and A. A. Penin, Nucl. Phys. **B563**, 200 (1999) [hep-ph/9907489].
- [59] S. Su and M. B. Wise, Phys. Lett. **B510**, 205 (2001) [hep-ph/0104169].

- [60] R. Harlander, M. Jezabek and J. H. Kühn, *Acta Phys. Polon.* **27**, 1781 (1996) [hep-ph/9506292].
- [61] S. Bethke, *J. Phys. G* **G26**, R27 (2000) [hep-ex/0004021].
- [62] I. Hinchliffe and A. V. Manohar, *Ann. Rev. Nucl. Part. Sci.* **50**, 643 (2000) [hep-ph/0004186];
- [63] P. N. Burrows et al. , in *Proceedings of 1996 DPF/DPB Snowmass Summer Study*, ed. D. Cassel et al. , (1997).
- [64] R. D. Heuer, D. J. Miller, F. Richard and P. M. Zerwas, hep-ph/0106315.
- [65] H. Baer, S. Dawson and L. Reina, *Phys. Rev.* **D61**, 013002 (2000) [hep-ph/9906419]; A. Juste and G. Merino, hep-ph/9910301.
- [66] R. J. Guth and J. H. Kühn, *Nucl. Phys.* **B368**, 38 (1992).
- [67] M. Jezabek and J. H. Kuhn, *Phys. Rev.* **D48**, 1910 (1993) [Erratum-ibid. **D49**, 4970 (1993)] [hep-ph/9302295].
- [68] A. H. Hoang, *Phys. Rev.* **D56**, 5851 (1997) [hep-ph/9704325].
- [69] C. Bauer and A. V. Manohar, *Phys. Rev.* **D57**, 337 (1998) [hep-ph/9708306]; B. Blok, J. G. Korner, D. Pirjol and J. C. Rojas, *Nucl. Phys.* **B496**, 358 (1997) [hep-ph/9607233].
- [70] A. Pineda and J. Soto, *Phys. Rev.* **D58**, 114011 (1998) [hep-ph/9802365].
- [71] B. A. Kniehl, A. A. Penin, M. Steinhauser and V. A. Smirnov, hep-ph/0106135.